DISSERTATION

NUMERICAL SIMULATIONS ON PATTERNS OF ALLUVIATION IN MIXED BEDROCK-ALLUVIAL CHANNELS

Submitted by

Jongseok Cho

Department of Civil and Environmental Engineering

In Partial fulfillment of the requirements

For the Degree of Doctor of Philosophy

Colorado State University

Fort Collins, Colorado

Spring 2023

Doctoral Committee:

Advisor: Peter A. Nelson

Pierre Y. Julien
Robert Ettema
Ellen E. Wohl

ABSTRACT

NUMERICAL SIMULATIONS ON PATTERNS OF ALLUVIATION

IN MIXED BEDROCK-ALLUVIAL CHANNELS

Mixed bedrock-alluvial rivers can exhibit partial alluvial cover, which may play an important role in controlling bedrock erosion rates and landscape evolution. However, numerical morphodynamic models generally are unable to predict the pattern of alluviation in these channels. Hence we present a new two-dimensional depth-averaged morphodynamic model that can be applied to both fully alluvial and mixed bedrock-alluvial channels, and we use the model to gain insight into the mechanisms responsible for the development of sediment patches and patterns of bedrock alluviation. The model computes hydrodynamics, sediment transport, and bed evolution, using a roughness partitioning that accounts for differential roughness of sediment and bedrock, roughness due to sediment transport, and form drag. The model successfully replicates observations of bar development and migration from a fully alluvial flume experiment, and it models persistent sediment patches observed in a mixed bedrock-alluvial flume experiment. Numerical experiments in which the form drag, sediment transport roughness, and ripple factor were neglected did not successfully reproduce the observed persistent sediment cover in the mixed bedrock-alluvial case, suggesting that accounting for these different roughness components is critical to successfully model sediment dynamics in bedrock channels.

Understanding the development and spatial distribution of alluvial patches in mixed bedrock-alluvial rivers is necessary to predict the mechanisms of the interactions between sediment transport, alluvial cover, and bedrock erosion. This study aims to analyze patterns of bedrock

alluviation using a 2D morphodynamic model, and to use the model results to better understand the mechanisms responsible for alluvial patterns that have been observed experimentally. A series of simulations are conducted to explore how alluvial patterns in mixed bedrock-alluvial channels form and evolve for different channel slopes and antecedent sediment layer thicknesses. In initially bare bedrock low-slope channels, the model predicts a linear relationship between sediment cover and sediment supply because areas of subcritical flow enable sediment deposition, while in steep-slope channels the flow remains fully supercritical and the model predicts so-called runaway alluviation in which the bedrock remains fully exposed at all sediment supplies below a threshold. For channels that are initially covered with sediment, the model predicts a slope-dependent sediment supply threshold above which a linear relationship between bedrock expo-sure and sediment supply develops, and below which the bedrock becomes fully exposed. For a given sediment supply, the fraction of bedrock exposure and average alluvial thickness converge toward the equilibrium value regardless of the initial cover thickness so long as it exceeds a minimum threshold. Steep channels are able to maintain a continuous strip of sediment under sub-capacity sediment supply conditions by achieving the balance between increased form drag as bedforms develop and reduced surface roughness as the portion of alluvial cover decreases. In lower-slope channels, alluvial patches are distributed sporadically in regions of the subcritical flow.

ACKNOWLEDGEMENTS

I would like to thank my advisor, Peter A. Nelson, for providing fundamental ideas, invaluable guidance, and research resources to complete this interesting study over the years.

I also appreciate my committee members, Drs. Pierre Julien, Robert Ettema, and Ellen Wohl helped expand my visions through the lectures and insightful discussions.

I am grateful for my adorable lifetime buddy, Doyeon.

Lastly, I sincerely appreciate my parents, Seongou and Kyungsook, and my sister Eunyung and her family for all their love and support.

TABLE OF CONTENTS

LIST OF TABLES

LIST OF FIGURES

CHAPTER 1

INTRODUCTION

River channels can be generally classified as either alluvial, bedrock, or mixed bedrock-alluvial (Figure 1.1) [Howard, 1980, 1987, 1998; Howard et al., 1994; Knighton, 2014]. The beds of alluvial rivers are entirely covered by the sediment of sufficient thickness that the underlying bedrock is not exposed [Sklar and Dietrich, 1998; Whipple, 2004]. In contrast, bedrock channels are characterized by frequently exposed bedrock and a lack of continuous alluvial cover in the channel bed and banks. Mixed bedrock-alluvial channels feature areas of exposed bedrock interspersed with patches of alluvial cover, potentially taking the form of alternate bars [e.g., Chatanantavet and Parker, 2008] or point bars at meander bends [Nittrouer et al., 2011; Nelson et al., 2014].

Channels with low sediment supply can erode alluvial material in the bed to the point where bedrock becomes exposed. River channel bedrock exposure is common in mountainous areas, where the river channel slope is steep and the flow velocity is high. The mixed bedrock-alluvial river channels are characterized by their excessive transport capacity compared to the in-channel sediment source and sediment supply rate from the surrounding environment.

The connection between sediment supply, sediment cover, and bedrock erosion are primary factors in understanding sediment transport mechanisms and the development of alluvial patches in mixed-bedrock alluvial channels. A theoretical framework of the saltation-abrasion model [Sklar and Dietrich, 2004] to predict bedrock erosion incorporates the erosional mechanisms of saltating bed load particles impacting and eroding bedrock [Sklar and Dietrich, 1998, 2001, 2004; Hartshorn et al., 2002; Demeter et al., 2005; Zhang et al., 2015].

Figure 1.1. Field photographs showing channel morphology. (a) alluvial channel [Booth and Bledsoe, 2009], (b) mixed bedrock-alluvial channel (Trail Canyon, Utah, U.S.) [Johnson et al., 2009], and (c) bedrock channel, (Hanase River, Kagoshima, Japan) [Inoue et al., 2014].

The saltation-abrasion model related erosion rate to sediment supply through the 'tools and cover' effect. The erosion rate is low at high sediment supply because the bedrock becomes 'covered' in alluvium. An alluvial deposit covering the bed protects the bedrock surface from abrasion and plucking processes produced by erosive forces of flow and sediment impact. The erosion rate is also low at low sediment supply because of lacking erosional 'tools.' The mobile grains actively collide with the exposed bedrock surface during the sediment transport processes by saltation and rolling.

Competition between the tools and cover effects controls the spatial distribution of bedrock erosion, resulting in lateral and vertical channel erosion and meandering [Finnegan et al., 2007; Turowski et al., 2007, 2008a, b; Lamb et al., 2015]. These coupled effects are introduced to develop mechanical bedrock erosion models where an increase in sediment flux intensifies the erosion rate, but then builds up a larger fraction of the alluvial layer reducing the erosion rate [Turowski and Rickenmann, 2009]. The cover effect is typically parameterized in models with linear or exponential relations where fractional bedrock exposure is a function of sediment supply to transport capacity ratio [Sklar and Dietrich, 1998, 2004; Turowski et al., 2007] (Figure 1.2).

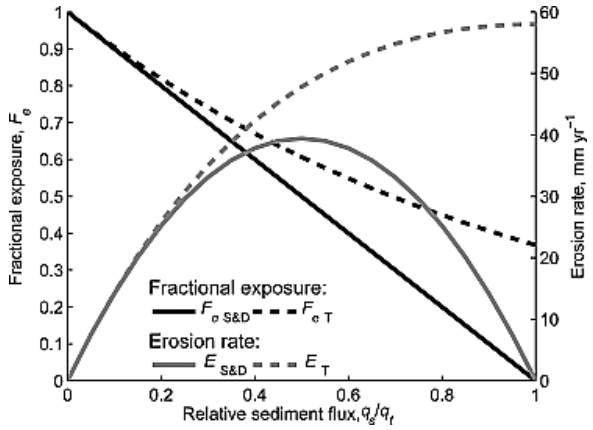

Figure 1.2. Relationships between fractional bedrock exposure (F_e), erosion rate (E), and relative sediment flux (q_s/q_c) as predicted by Sklar and Dietrich [2004] and Turowski et al. [2007]. For the latter curve, $\varphi = 1$. E is calculated as by Sklar and Dietrich [2004]. Hodge and Hoey [2012]

Accurate prediction of the spatial pattern of alluvial cover in mixed bedrock-alluvial channels is critical for modeling their patterns of erosion and evolution.

Experiments and modeling have demonstrated the dynamic relationship between the development of alluvial cover in mixed bedrock-alluvial channels and the erosion and evolution of the channel. Experiments have shown that sediment tends to collect within potholes [Goode and Wohl, 2010a, b] and along the bottom of the incised inner bedrock channel [Finnegan et al., 2007; Johnson and Whipple, 2007] (Figure 1.3). Meanwhile, the loose material is transported through preferential routes [Nelson and Seminara, 2012], implying lateral erosion primarily at the higher area of the bed and potential channel widening [Nelson and Seminara, 2011] (Figure 1.4a). In some experiments, multiple sediment transport pathways have formed erosional longitudinal grooves [Inoue et al., 2016; Inoue and Nelson, 2020]. The longitudinal grooves with high sediment concentration underwent widening and merging with adjacent grooves over time (Figure 1.4b).

Bedrock channels play a critical role in the evolution of landscapes [Seidl and Dietrich, 1992; Wohl, 1993; Howard et al., 1994; Tinkler and Wohl, 1998; Whipple and Tucker, 2002; Gasparini et al., 2007; Hodge and Hoey, 2012]. Bedrock channels provide a lower boundary

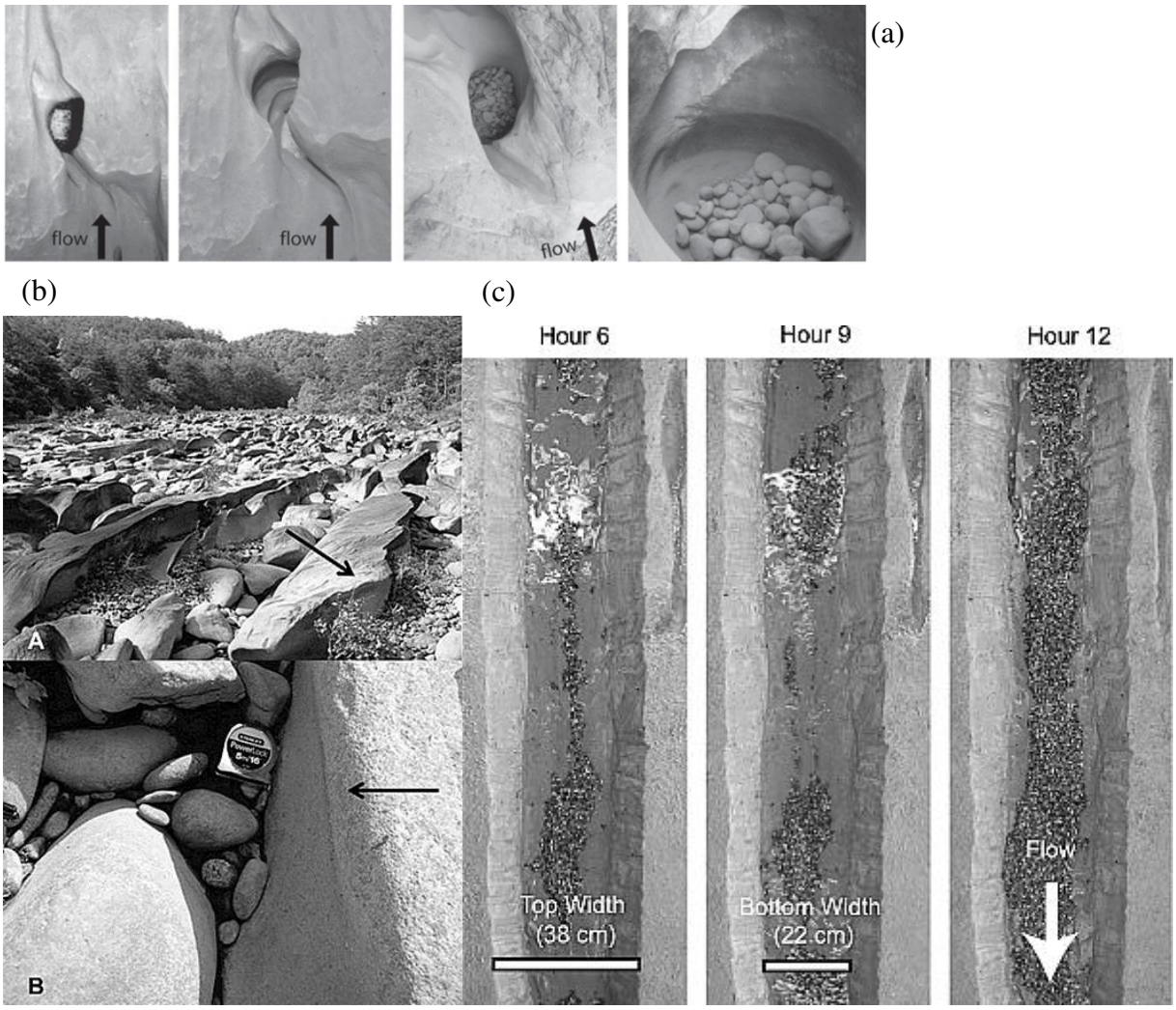

Figure 1.3. Sediment deposition in bedrock channel (a) within potholes [Johnson and Whipple, 2007], (b) between the bedrock ribs [Goode and Wohl, 2010], and (c) bottom of the incised inner bedrock channel [Finnegan et al., 2007].

condition by determining the landscape denudation rate and conveying climatic and tectonic perturbation signals for the rest of the landscapes [Whipple and Tucker, 1999; Whipple, 2001]. Given the direct connection between patterns of alluvial sediment in the channel and the local erosion rate, an improved understanding of the dynamics of alluviation in mixed bedrock-alluvial rivers can lead to better landscape evolution models and a better understanding of the dynamics of the overall landscape.

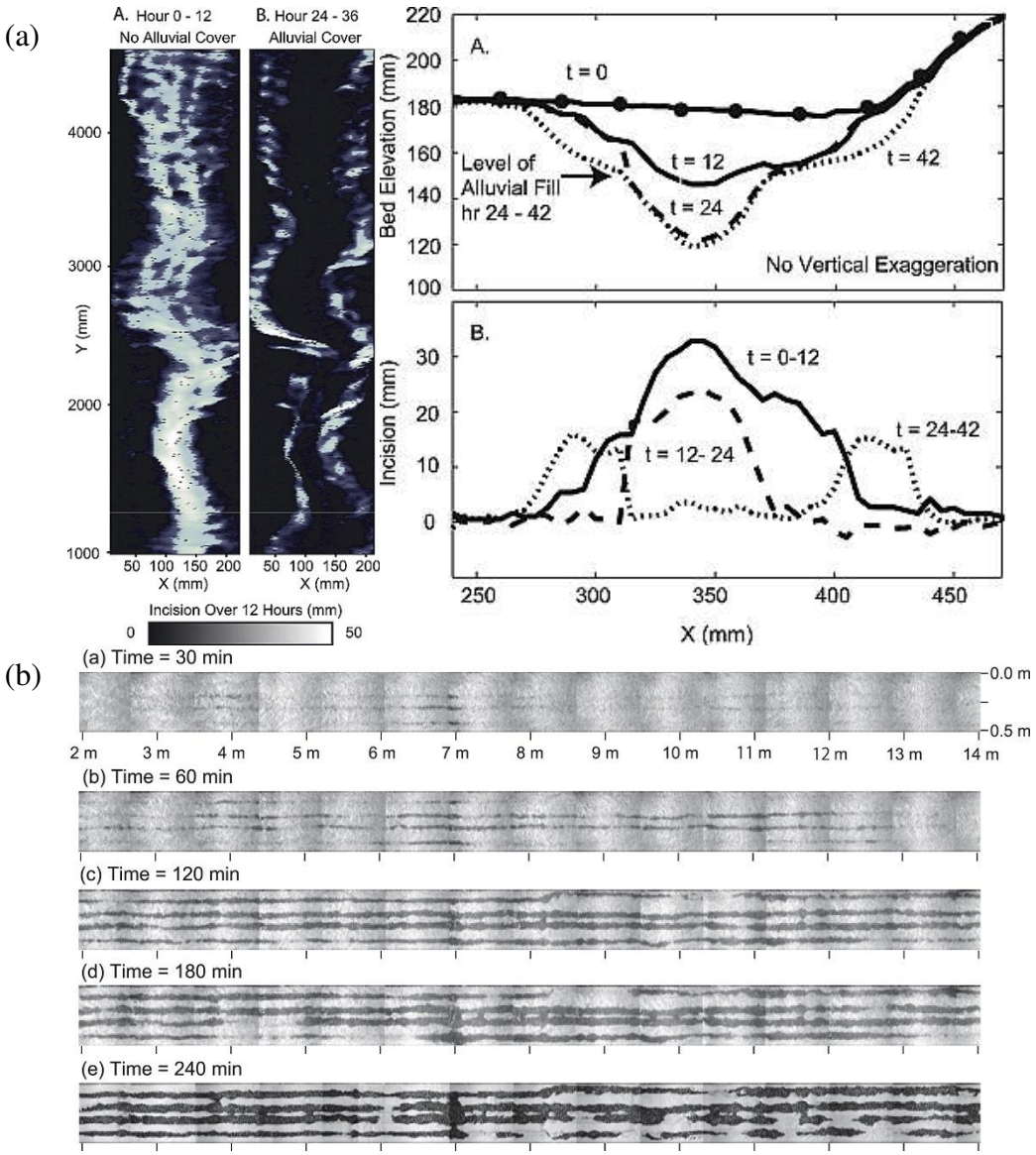

Figure 1.4. Bedrock channel evolution (a) channel widening [Finnegan et al., 2007] and (b) longitudinal groove widening and merging [Inoue and Nelson, 2020].

Observations from flume experiments documenting the development of alluvial cover patterns on bedrock beds have provided important insight into the dynamics of alluviation and raised important questions which help to motivate this study. Chatanantavet and Parker [2008] conducted a series of experiments in a straight flume where they varied the rate of sediment supply, the initial cover of sediment on the bed, the slope, and the grain size. Hodge and Hoey [2016a, b] performed

experiments in a 3D printed scale model of a jointed limestone bedrock river in which the patterns of sediment deposits at different sediment supply rates were documented. Mishra and Inoue [2020] performed flume experiments with varying bedrock roughness using different patterns of bedrock configuration. These experiments have documented a range of dynamic behavior in mixed bedrock-alluvial rivers, where the location and amount of sediment cover are impacted by variables such as the flow rate, sediment supply rate and grain size, channel slope, bedrock topography, and antecedent bed sediment condition.

Given the range of observations from these flume experiments, a successful morphodynamic model should be able to predict patterns of alluvial cover in a wide range of channel slopes, variable initial alluvial thickness, spatial variation of local bed topography and flow velocity, differential alluvial and bedrock roughness, and bed evolution with alternate bar development. Thus far, morphodynamic models have been largely unsuccessful in replicating experimental observations, especially the development of persistent patches of sediment cover under sustained sediment supply deficit. Among the more successful models, Hodge and Hoey [2012] developed a cellular automaton model to simulate sediment transport in bedrock channels using different values of grain entrainment probabilities in bedrock and alluvial surfaces. They replicated some of the dynamics observed in the experiments by Chatanantavet and Parker [2008]. A macro-roughness-based model [Zhang et al., 2015] exhibited sediment stripping from the alluvial channel and the bare bedrock bed emplacement. Inoue et al. [2016] presented a numerical prediction of bed evolution and alternate bar formation.

Despite these recent advances in modeling the morphodynamics of mixed bedrock-alluvial rivers, there remain uncertainties about how different sediment and bedrock roughness influences sediment dynamics, what controls the development of bars and bedforms in mixed bedrock-

alluvial rivers, and how hydraulic features interact to potentially control alluvial patterns. Existing models cannot resolve these issues because they are one-dimensional and unable to predict bars and bedforms, or they do not fully account for roughness feedback depending on local sediment cover. For example, current models of mixed bedrock-alluvial morphodynamics have not fully replicated the relationship between overall sediment cover and the sediment supply to capacity ratio, or the development of alternate bars as reported in Chatanantavet and Parker [2008] (Figure 1.5).

This study intends to resolve these limitations by developing a new numerical model for mixed bedrock-alluvial morphodynamics that includes: (1) a multi-dimensional approach to account for the influence of potential 3D bedforms (e.g., alternate bars, antidunes, and dunes) in a straight channel; (2) the effect of flow resistance partitioned into skin friction due to particles and

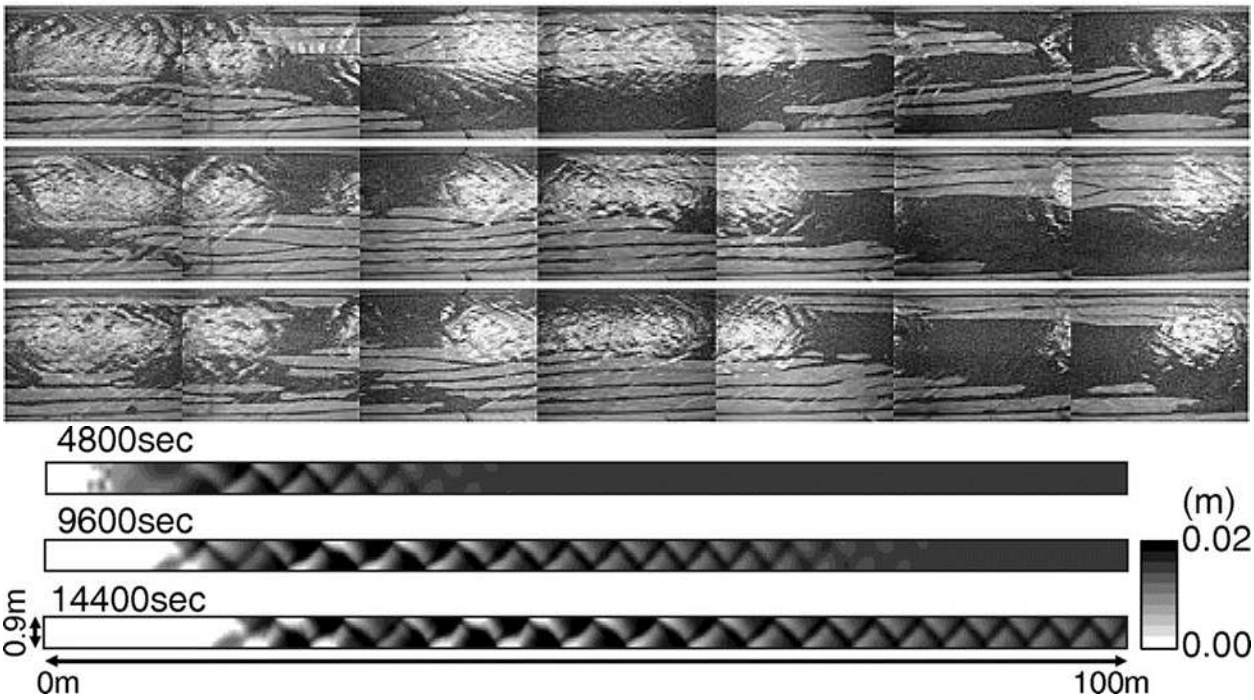

Figure 1.5. Evolution of alluvial layer in mixed bedrock alluvial channels from (top) Run 1-A2 of Chatanantavet and Parker [2008] flume experiment in 13 m long channel at 1.25, 2.25, and 4.25 hours from top to bottom and (bottom) corresponding numerical prediction from Inoue et al. [2016]. The dark and light area indicate sediment and bedrock surface, respectively. The numerical model predicts the washout of alluvial material from upstream to downstream.

bedrock surface roughness, bed load transport roughness accounting for near-bed sediment transport, and form drag associated with dimensions of alluvial cover and irregular bedrock topography; (3) application of the ripple factor to take into account for an intermediate state between the planar bed and small-scale bedforms. The model also incorporates recent advances in characterizing sediment continuity for bedrock-alluvial rivers, and it uses a shock-capturing numerical scheme that maintains stability across subcritical and supercritical flows.

In this dissertation, Chapter 2 fully describes the new numerical model and tests it against benchmark observations collected in fully alluvial and mixed bedrock-alluvial flume experiments. The model is shown to successfully simulate observations for both experiments. Furthermore, numerical simulations where the roughness submodels for form drag, transport roughness, and the ripple factor are neglected are shown to produce incorrect results, indicating the importance of fully accounting for each form of roughness when modeling conditions in mixed bedrock-alluvial rivers.

In Chapter 3, the model is used to gain further insight on the dynamics of alluvial patterns in mixed bedrock-alluvial channels. In order to investigate what controls morphological processes in mixed bedrock-alluvial channels, we explore the effect of different channel characteristics, such as channel slope, presence and absence of initial alluvial cover, and antecedent alluvial layer thickness, with varying sediment supply rates. These simulations replicate, for the first time, observations collected in mixed bedrock-alluvial flume experiments, and provide mechanistic explanations for the relationships between sediment cover and sediment supply.

CHAPTER 2

NUMERICAL MODELING PATTERNS OF ALLUVIATION IN MIXED BED-ROCK-ALLUVIAL CHANNELS

2.1. Introduction

River channels can be classified as either alluvial, bedrock, or mixed bedrock-alluvial [Howard, 1980, 1987, 1998; Howard et al., 1994; Knighton, 2014]. The beds of alluvial rivers are entirely covered by sediment of sufficient thickness so that the underlying bedrock is not exposed [Tinkler and Wohl, 1998; Whipple, 2004]. In contrast, bedrock channels are characterized by frequently exposed bedrock and a lack of continuous alluvial cover in the channel bed and banks. Mixed bedrock-alluvial channels tend to have sediment supply that is less than their sediment transport capacity, and they feature the exposed bedrock interspersed with patches of alluvial cover, potentially taking the form of alternate bars [e.g., Chatanantavet & Parker, 2008] or point bars at meander bends [Nittrouer et al., 2011; Nelson et al., 2014].

The pattern of alluvial cover in mixed bedrock-alluvial channels likely plays a role in the morphological evolution of those channels, and consequently on landscape evolution [Seidl and Dietrich, 1992; Wohl, 1993; Howard et al., 1994; Tinkler and Wohl, 1998; Whipple and Tucker, 2002; Gasparini et al., 2007; Hodge and Hoey, 2012]. Bedrock channel erosion sets the lower boundary condition for landscape evolution and bedrock channels convey climatic and tectonic perturbation through the landscape [Whipple and Tucker, 1999; Whipple, 2001]. Alluvial cover is an important component of mechanistic models of bedrock erosion; for example, the saltation-abrasion model incorporates the erosional mechanism of saltating bed load particles impacting and eroding bedrock [Sklar and Dietrich, 1998, 2001, 2004; Hartshorn et al., 2002; Demeter et al.,

2005; Zhang et al., 2015]. Competition between the tools and cover effects controls the spatial distribution of the bedrock channel erosion that results in lateral and vertical channel erosion and meandering [Finnegan et al., 2007; Turowski et al., 2008a, b, 2007; Lamb et al., 2015].

Observations from flume experiments documenting the development of alluvial cover patterns on bedrock beds have shown that alluvial cover in these channels depends on channel slope, the initial thickness of alluvial sediment, sediment supply, bedrock roughness, and channel topography. Chatanantavet and Parker [2008] conducted a series of experiments in a straight flume where they varied the rate of sediment supply, the initial cover of sediment on the bed, the slope, and the grain size. Their experiments illuminated several exciting phenomena in mixed bedrock-alluvial channels. First, the pattern and trajectory of the alluvial cover appear to be slope-dependent, wherein at low slopes ($S = 0.0115$) the exposed bed fraction linearly decreases with increasing sediment supply, akin to the linear relationship hypothesized by Sklar and Dietrich [2004]. However, at higher slopes ($S = 0.02$), experiments starting with a bare bed did not develop persistent alluvial cover at any supplied rate until that rate exceeded the overall transport capacity of the channel. At that point, "runaway alluviation" occurred, and the entire channel became covered in sediment. Second, the thickness of the initial alluvial cover affected the dynamics of alluviation on the bed, wherein at low initial alluvial thickness the bed was stripped clean, whereas thicker initial sediment covers eventually reached a non-zero fraction of bedrock exposure. Third, some of their experiments developed continuous strips of sediment moving from one side of the channel to the other, akin to alternate bars.

Mishra and Inoue [2020] performed flume experiments with varying bedrock roughness. Plotting the extent of alluvial cover, they observed against sediment supply shows a positive correlation when the hydraulic roughness of the bedrock bed is larger than that of the alluvial surface.

However, a sudden transition from bare bedrock bed to full alluviation was observed as sediment supply momentarily exceeded the channel's transport capacity when the ratio of hydraulic roughness height of bedrock to grain size (k_{sb}/d) is 1.9 or lower. They also proposed an approximation of dimensionless critical shear stress for incipient particle motion over bedrock beds as a function of relative roughness height.

Hodge and Hoey [2016a, b] performed experiments in a 3D printed scale model of a jointed limestone bedrock river in which the patterns of sediment deposits at different sediment supply rates were documented. Their experiments pointed out the importance of bedrock topography on depositional patterns, as patches of sediment tended to form in the lowest portions of the bed, and at higher discharge and sediment supply, the bed topography played a less important role than sediment-sediment and sediment-flow interactions in stabilizing patches of alluvium.

Numerical models of sediment transport and bed evolution in mixed bedrock-alluvial channels have struggled to capture the dynamics of alluvial cover observed in experiments or in the field. Morphodynamic models simulate river channel evolution by iteratively using hydraulic flow field calculations to estimate sediment transport rates, which are then used in the conservation of sediment mass (i.e., the Exner equation) to calculate bed erosion and deposition patterns. These types of models have been used for decades to understand the dynamics of alluvial rivers, such as the development and migration of alternate bars [e.g., Defina, 2003; Bernini et al., 2006; Qian et al., 2017], sediment sorting [e.g., Nelson et al., 2015a, b], braiding [e.g., Murray and Paola, 1997; Schuurman et al., 2013], meandering [e.g., Smith and Mclean, 1984; Nelson et al., 2003], and armoring [e.g., Parker and Klingeman, 1982; Parker and Toro-Escobar, 2002]. However, alluvial morphodynamic models generally assume that the sediment supply equals or exceeds the sediment transport capacity, which is not the case for mixed bedrock-alluvial rivers.

This assumption has only recently begun to be relaxed in attempts to use morphodynamic models to better understand mixed bedrock-alluvial rivers [e.g., Nelson and Seminara, 2012]. Using a cellular automaton model governed by probabilities of individual grain movement, Hodge and Hoey [2012] studied the relationship between the fraction of bedrock exposure and the ratio of sediment supply to capacity on noneroding bedrock beds. Zhang et al. [2015] expressed bedrock cover fraction as a ratio of vertical length scale between alluvial thickness and macro-roughness of bedrock topography representing the statistical characteristics of bedrock surface fluctuations. This MRSAA (macro-roughness saltation-abrasion-alluviation) model was later implemented to investigate the knickpoint migration [Zhang et al., 2018; 2019] and formation of the cyclic steps [Izumi et al., 2017] to spatiotemporal variation of sediment supply. Inoue et al. [2016] provided an early attempt to investigate alternate bar formation and bedrock incision in mixed bedrock-alluvial channels in response to the different ratio of sediment supply to channel's transport capacity.

Larger-than-grain-scale bedrock topography, sometimes called "macrotopography", has recently been incorporated into one-dimensional morphodynamic models [Zhang et al., 2015]. The model solutions for alluvial response to sediment supply show that stripping of antecedent sediment from upstream to downstream occurs with the termination of sediment supply, and the development of an alluvial layer with a thickness corresponding to the ratio of sediment supply to transport capacity (q_s/q_c), which propagates downstream over bare bedrock when the sediment supply is increased. Application of nonlinear wave speed to the alluvial layer predicted that alluvium over a bedrock surface with a small cover fraction migrated downstream much faster than those consisting of a higher fraction cover.

Despite these recent advances in modeling the morphodynamics of mixed bedrock-alluvial rivers, there remain uncertainties about how different sediment and bedrock roughness influences sediment dynamics, what controls the development of bars and bedforms in mixed bedrock-alluvial rivers, and how hydraulics and macroroughness features interact to control alluvial patterns. Existing models are not able to resolve these issues because either they are one-dimensional and unable to predict bars and bedforms, they do not fully account for roughness feedback depending on local sediment cover, or the impact of hydraulic parameters including slope, roughness, and shear stress on sediment transport are unclear. For example, current models of mixed bedrock-alluvial morphodynamics have not been able to fully replicate the relationship between overall sediment cover and the sediment supply to capacity ratio or the development of alternate bars, as reported in Chatanantavet and Parker [2008].

We still generally do not have the ability to use morphodynamic models to predict patterns of alluvial cover in mixed bedrock-alluvial channels or the dynamics of alternate bars in mixed bedrock-alluvial channels. One reason we lack these modeling tools may be our general lack of understanding of the effects of hydraulic parameters, such as the importance of hydraulic resistance of alluvial patches and the consequent feedback on sediment transport and alluviation. We hypothesize that accounting for differential bedrock and sediment roughness, roughness from sediment transport, form drag, and a near-bed shear stress correction are necessary to capture sediment dynamics in mixed bedrock-alluvial channels.

This study intends to resolve the limitations models encounter when attempting to simulate sediment dynamics in a mixed bedrock-alluvial channel by developing a new model that uses: (1) a two-dimensional approach to account for the influence of potential bedforms (e.g., alternate bars, antidunes, and dunes) in a straight channel; (2) the effect of flow resistance partitioned into skin

friction due to stationary particles and bedrock surface roughness, form drag associated with dimensions of alluvial cover and irregular bedrock topography, and bed load roughness produced by saltating sediment; (3) application of a ripple factor to take into account for an intermediate state between the planar bed and small-scale bedforms. The model also must be able to simulate supercritical, subcritical, and transcritical flows, which often occur in bedrock channels [e.g., Tinkler and Wohl, 1998; Kostic et al., 2010].

We use two experiments to demonstrate that our model can reproduce observations made in fully alluvial and mixed bedrock-alluvial channels, and we explore the impact of eliminating some roughness terms on mixed bedrock-alluvial dynamics and predictions of the alluvial cover. To do so, we simulate an experiment of Lanzoni [2000a] for alternate bar formation in an alluvial channel and an experiment of Chatanantavet and Parker [2008] for gravel patch development in a mixed bedrock-alluvial channel to assess model performance. Our model successfully replicates sediment dynamics in both experiments. The numerical experiments that neglect form drag and transport components of the roughness do not reproduce observations from the Chatanantavet and Parker [2008] experiment, indicating that those components play a critical role in mixed bedrock-alluvial sediment dynamics.

2.2. Morphodynamic model

We have developed a new morphodynamic model that simulates sediment transport and deposition in mixed bedrock-alluvial channels. The model used in this study consists of three components: a hydrodynamic model describing the depth-averaged flow field, a sediment transport model describing bed load sediment transport rate, and a bed evolution model updating bed elevation and the areal fraction of bedrock cover. Unlike previous models of mixed bedrock-alluvial

morphodynamics, this new model accounts for form drag and sediment transport roughness, in addition to surface (grain and bedrock) roughness and a roughness-dependent critical Shields stress. In addition, the total shear stress is corrected with a ripple factor in the sediment transport model, as the bedform drag does not contribute to the bed load transport.

2.2.1. Flow model

The governing equations for calculating flow depth and velocity are composed of the depth-averaged form of mass continuity and momentum balance in a 2D Cartesian coordinate system:

$$\frac{\partial Q}{\partial t}+\frac{\partial F_x}{\partial x}+\frac{\partial F_y}{\partial y}=\frac{\partial D_x}{\partial x}+\frac{\partial D_y}{\partial y}+S_b+S_f\,, \tag{2.1}$$

where t is time, x and y are Cartesian coordinates, Q are the conservative variables, F_x and F_y are the convective fluxes, D_x and D_y are the diffusive fluxes, S_b are the bed slope terms, and S_f are the friction slope:

$$Q=\begin{bmatrix} h \\ hu \\ hv \end{bmatrix},\quad F_x=\begin{bmatrix} hu \\ huu+\frac{1}{2}g(h^2-z_b^2) \\ hvu \end{bmatrix},\quad F_y=\begin{bmatrix} hv \\ huv \\ hvv+\frac{1}{2}g(h^2-z_b^2) \end{bmatrix},$$

$$D_x=\begin{bmatrix} 0 \\ 2h(\nu+\nu_t)\frac{\partial u}{\partial x} \\ h(\nu+\nu_t)\left(\frac{\partial u}{\partial y}+\frac{\partial v}{\partial x}\right) \end{bmatrix},\quad D_y=\begin{bmatrix} 0 \\ h(\nu+\nu_t)\left(\frac{\partial u}{\partial y}+\frac{\partial v}{\partial x}\right) \\ 2h(\nu+\nu_t)\frac{\partial v}{\partial y} \end{bmatrix}, \tag{2.2}$$

$$S_b=\begin{bmatrix} 0 \\ -g\eta\frac{\partial z_b}{\partial x} \\ -g\eta\frac{\partial z_b}{\partial y} \end{bmatrix},\quad S_f=\begin{bmatrix} 0 \\ -\frac{\tau_{bx}}{\rho} \\ -\frac{\tau_{by}}{\rho} \end{bmatrix},$$

where h is the flow depth, u and v are the velocities in x- and y-directions, respectively, g is the gravitational acceleration, ν and ν_t are the kinematic viscosity of water and the turbulent eddy viscosity, respectively, η is the water surface elevation, z_b is the bed elevation, and ρ is the density of water. The bed shear stresses τ_{bx} and τ_{by} in x- and y-direction are given by

$$\left(\tau_{bx}, \tau_{by}\right) = \rho C_f \sqrt{u^2 + v^2}(u, v)\,, \tag{2.3}$$

where C_f is a friction coefficient estimated using the law of the wall as a function of the flow depth h and total roughness height k_0:

$$C_f = \left[6 + 2.5 \ln\left(\frac{h}{k_0}\right)\right]^{-2}. \tag{2.4}$$

2.2.2. The depth-averaged mixing-length model

The calculation of the turbulent viscosity term is based on a mixing-length model with depth-averaged terms developed by Stansby [2003]:

$$\nu_t = \sqrt{l_h^4 \left[2\left(\frac{\partial u}{\partial x}\right)^2 + 2\left(\frac{\partial v}{\partial y}\right)^2 + \left(\frac{\partial v}{\partial x} + \frac{\partial u}{\partial y}\right)^2\right] + (\gamma u_* h)^2}\,, \tag{2.5}$$

where l_h is a horizontal mixing length scale ($l_h \approx 0.267\kappa h$), κ is the von Karman constant ($\kappa \approx 0.408$), and γ is a constant that accounts for vertical mixing ($\gamma \approx 0.067$). u_* is the local shear velocity;

$$u_* = \sqrt{\tau_b/\rho}\,, \tag{2.6}$$

where $\tau_b = \sqrt{\tau_{bx}^2 + \tau_{by}^2}$ is the local bed shear stress vector, with components τ_{bx} and τ_{by} in the *x*- and *y*-directions, respectively.

2.2.3. Bed roughness

The total roughness height k_0 is partitioned into three fractional roughness components, including skin friction k_s, form drag k_f, and bed load transport k_t:

$$k_0 = k_s + k_f + k_t \,. \tag{2.7}$$

The skin friction is induced by the viscous shear stress and pressure force acting on the individual grains on the bed, and it relates to the size of the bed material. The local skin friction roughness height varies with surface particle size in the completely alluvial channel and the degree of irregularity of the bed surface in the bedrock channel. The calculation of skin friction in the mixed bedrock-alluvial channel is based on the assumption that the skin friction is linearly associated with the changes in the fraction of bedrock covered by alluvium:

$$k_s = P_c k_{sa} + (1 - P_c) k_{sb} \tag{2.8}$$

where k_{sa} and k_{sb} are the hydraulic roughness height of the alluvial bed and bedrock bed, respectively. The local areal fraction of alluvial cover $P_c = \min[\eta_a / C_m \,, 1]$, in which $C_m = \pi d/6$ is the maximum volume of monolayer that spherical sediment grains of constant diameter d are uniformly distributed over the bed surface [Nelson and Seminara, 2012] and η_a is the thickness of the alluvial layer.

The form drag component of roughness results from the pressure force acting over entire bedforms and is not responsible for the bed load motion of sediment particles [Maddux et al., 2003a, b]. We calculate the form drag component of roughness as a function of bed morphology through the empirical relation of Grant and Madsen [1982]:

$$k_f = 30 a_r \frac{\eta_r^2}{\lambda_r} \tag{2.9}$$

where η_r and λ_r are bed form height and wavelength, and a_r is a coefficient in the range from 0.3 to 3. Grant and Madsen [1982] suggested $a_r = 0.923$.

For the sediment transport component of roughness, Wiberg and Rubin [1989] proposed for the flat bed condition:

$$k_t = 30\alpha_{ws} d \frac{a_1 T_*}{1 + a_2 T_*} \tag{2.10}$$

where $T_* = \tau^*/\tau_c^*$ is the transport stage, τ^* is the dimensionless shear stress, τ_c^* is the critical dimensionless Shields stress, $a_1 = 0.68$, $a_2 = 0.0204(\ln 100d)^2 + 0.0220(\ln 100d) + 0.0709$, and $\alpha_{ws} = 0.056$. Here, the effect of local variation of bed topography is applied to the bed shear stress to account for the gravity effect.

2.2.4. Bed deformation model

The local volumetric concentration of sediment per unit area is calculated using the sediment conservation model for mixed bedrock-alluvial channel beds proposed by Luu et al. [2004]:

$$\frac{\partial V_{ba}}{\partial t} + \frac{\partial q_{bx}}{\partial x} + \frac{\partial q_{by}}{\partial y} = 0\,, \tag{2.11}$$

where V_{ba} is the total volume of sediment per unit area and q_{bx} and q_{by} are vectors of the bed load transport rate per unit width in the x- and y-directions, respectively. The thickness of the alluvial layer η_a and the volume of sediment in the bed load layer V_b are separately updated considering the saturation volume of the bed load layer V_{bc}. This saturation volume is a threshold value that determines whether the particles deposit on the bed or rapidly saltate over the surface without resting on the bed. When V_{ba} exceeds V_{bc}, a volume of sediment equal to the difference between V_{ba} and V_{bc} deposits on the bed as an alluvial layer. When V_{ba} is less than V_{bc}, the particles pass over the bedrock surface as throughput load without deposition:

$$\eta_a = \begin{cases} \dfrac{V_{ba} - V_{bc}}{1 - \lambda} & \text{for} \quad V_{bc} \le V_{ba} \\ 0 & \text{for} \quad 0 \le V_{ba} < V_{bc} \end{cases} \tag{2.12}$$

where λ represents the porosity of the bed and V_{bc} is the saturation volume of the bed load layer per unit area. When the bedrock is wholly exposed ($\eta_a = 0$), the volume of the throughput bed load layer is lower than the saturation volume. When the bed is partially or fully covered with sediment ($\eta_a > 0$), V_b equates to V_{bc} because sediment particles exchange occurs between alluvial and bed load layers:

$$V_b = \begin{cases} V_{bc} & \text{for} \quad V_{bc} \leq V_{ba} \\ V_{ba} & \text{for} \quad 0 \leq V_{ba} < V_{bc} \end{cases}. \tag{2.13}$$

The saturation volume of bed load per unit area V_{bc} is defined by

$$V_{bc} = \frac{q_{bc}}{u_s}, \tag{2.14}$$

where q_{bc} is the bed load transport capacity per unit width and u_s is the saltation velocity, calculated here with the empirical excess shear stress relation presented in [Sklar and Dietrich, 2004]:

$$\frac{u_s}{\sqrt{R_b g d}} = 1.56\left(\frac{\tau^*}{\tau_c^*} - 1\right)^{0.56}, \tag{2.15}$$

where $R_b = (\rho_s - \rho)/\rho$ denotes submerged specific gravity of sediment and ρ_s is the density of the sediment. The bed load transport capacity per unit width q_{bc} is estimated using the relation based on Ashida and Michiue [1972]:

$$\frac{q_{bc}}{\sqrt{R_b g d^3}} = 17\left(\sqrt{\mu\tau^*} - \sqrt{\tau_c^*}\right)(\mu\tau^* - \tau_c^*) \tag{2.16}$$

where dimensionless shear stress τ^* is defined as

$$\tau^* = \frac{\tau_b}{\rho R_b g d} \tag{2.17}$$

and $\mu \leq 1$ is the ripple factor, the ratio of the grain roughness to bed roughness [Ribberink, 1987] (discussed further in Section 2.2.5).

The volumetric sediment transport rate per unit width in x- and y-direction is denoted

$$\left(q_{bx}, q_{by}\right) = q_b(\cos\alpha\,, \sin\alpha) \tag{2.18}$$

where α is the angle of bed load transport and the sediment transport intensity, q_b, depends on the ratio of the volume of sediment and its saturation value. The bed load transport rate in bedrock with a sufficient local volume of sediment equals the sediment transport capacity. However, in bedrock rivers without sediment cover, the bed load transport rate is less than the bed load transport capacity:

$$q_b = \begin{cases} \dfrac{V_b}{V_{bc}} q_{bc} & \text{for} \quad 0 \le V_b < V_{bc} \\ q_{bc} & \text{for} \quad V_{bc} \le V_b \end{cases}. \tag{2.19}$$

When considering the effect of gravity acting on particles for gradually varying bed elevation, the sediment transport direction deviates from the direction of the boundary shear stress. Here we adopt the well-known relationship [Struiksma, 1985]:

$$\tan\alpha = \frac{\sin\delta - \dfrac{1}{\mathrm{f}(\tau^*)}\dfrac{\partial z_b}{\partial y}}{\cos\delta - \dfrac{1}{\mathrm{f}(\tau^*)}\dfrac{\partial z_b}{\partial x}}, \tag{2.20}$$

where δ is the near-bed flow direction estimated to account for the influence of spiral water motion induced by bed topography as

$$\delta = \tan^{-1}\left(\frac{v}{u}\right) - \tan^{-1}\left(A\frac{h}{r_s}\right), \tag{2.21}$$

where the local radius of depth-averaged stream curvature is

$$r_s = \frac{U^3}{u^2\dfrac{\partial v}{\partial x} + uv\left(\dfrac{\partial v}{\partial y} - \dfrac{\partial u}{\partial x}\right) - v^2\dfrac{\partial u}{\partial y}}, \tag{2.22}$$

where $U = \sqrt{u^2 + v^2}$ is the local flow velocity and the coefficient weighting the intensity of helical flow is

$$A = \frac{2}{\kappa^2}\left(1 - \frac{\sqrt{C_f}}{\kappa}\right), \tag{2.23}$$

and $f(\tau^*)$ is a function weighting the influence of the bed slope, following the form proposed by Talmon et al. [1995]:

$$f(\tau^*) = 9\left(\frac{d}{h}\right)^{0.3}\sqrt{\tau^*}\,. \tag{2.24}$$

2.2.5. Ripple factor

The bed load sediment transport rate is expressed as a function of shear stress acting over the channel bed. The presence of bedforms leads to a partial reduction of the total shear stress related to the form drag, and the remainder is available for sediment transport. The Meyer-Peter and Muller [1948] sediment transport relation accounted for the ripple roughness by correcting the dimensionless shear stress with the ripple factor. Subsequently, several models for estimating the ripple factor have been proposed as a function of the skin friction relative to the total friction [Vermeer, 1986; Ribberink, 1987]:

$$\mu = \left(\frac{C_{fs}}{C_f}\right)^{n/2} \tag{2.25}$$

where C_{fs} is the friction coefficient accounting for skin friction obtained by substituting k_0 with $k_s + k_t$ in equation (2.4), and the exponent n is defined by

$$n = 1.8 + 0.27\log q^* \tag{2.26}$$

where $q^* = q_{bc}/\sqrt{R_b g d^3}$ is the dimensionless bed load transport rate. This relationship is valid for $0.001 \leq q^* \leq 1$ [Vermeer, 1986].

2.2.6. Critical dimensionless Shields stress

Flume experiments conducted in bedrock channels [Inoue et al., 2014; Mishra and Inoue, 2020] have related the channel roughness and dimensionless critical shear stress of sediment movement. A power approximation proposed by Mishra and Inoue [2020] is applied to this model to take into account the effect of total hydraulic roughness on critical shear stress:

$$\tau_{c0}^{*} = \tau_{c\alpha}^{*}(k_0/d)^{0.6} \tag{2.27}$$

where $\tau_{c\alpha}^{*}$ is the critical Shields stress back-calculated from sediment transport capacity measured from the experiment in the flat channel. In addition to the bed roughness, the local bed slope effect on the initiation of particle motion can be added because the local bed slope provides a gravitational component of the force exerted on the particle [Soulsby, 1997; Duan and Julien, 2005]:

$$\frac{\tau_c^{*}}{\tau_{c0}^{*}} = \frac{\sin(\phi + \beta_s)}{\sin\phi}\frac{\cos\beta_n}{\sqrt{1 - \tan^2\beta_n/\tan^2\phi}} \tag{2.28}$$

where ϕ is the grain angle of repose and β_s and β_n are the slope in the streamwise and cross-stream direction of the sediment transport, respectively. A simple approach was proposed by Wiberg and Smith [1987] for the treatment of heterogeneous bed conditions through the geometric relation of friction angle as a function of particle size to the roughness length scale of the bed:

$$\phi = \cos^{-1}\left(\frac{d/k_s - 0.02}{d/k_s + 1}\right). \tag{2.29}$$

The bed slopes in the streamwise and cross-stream directions are

$$\beta_s = \tan^{-1}\left(\frac{\partial z}{\partial x}\cos\alpha + \frac{\partial z}{\partial y}\sin\alpha\right), \beta_n = \tan^{-1}\left(\frac{\partial z}{\partial y}\cos\alpha - \frac{\partial z}{\partial x}\sin\alpha\right). \tag{2.30}$$

2.2.7. Solution procedure

The morphodynamic model calculates the flow field variables, sediment transport rate, and bed elevation. The model uses a decoupled approximation of the morphodynamic system by assuming that the response time of the bed evolution is relatively long compared to the time scale of the hydraulic processes [De Vries, 1965; Nelson and Smith, 1989; Nelson, 1990; Defina, 2003]. Therefore the hydrodynamic solver is followed by the calculation of the modified Exner equation.

First, local water depth and flow velocity are calculated using the hydrodynamic model (equation (2.1) - (2.2)). The friction term is estimated by taking into account the roughness of the bedrock (k_{sb}) and alluvial surfaces (k_{sa}), topographic variability (k_f), and the effect of saltating grains during sediment transport (k_t). Flow-conservative variables (h, hu, and hv) at each cell interface are calculated using the total variation diminishing (TVD) scheme [Toro, 2009] for cell-centered advection terms (F_x and F_y).

Second, the local sediment transport rate (q_b) is estimated considering the local circumstance of sediment deposition, which is determined by the fraction of bedrock cover (P_c) (equation (2.14) - (2.16)). The depth-averaged flow variables (h, u, v, and k_s) determine the threshold of incipient sediment motion (τ^* and τ_c^*), then the local bed load transport rate (q_b), grain saltation velocity (u_s), and saturation volume of the bed load layer (V_{bc}) are calculated.

Third, the sediment flux divergence updates the total sediment volume per unit area (equation (2.11)). Finally, the new alluvial layer thickness (η_a) and the volume of bed load transport per unit area (V_b) are determined by whether the bedrock is covered by alluvium or exposed (equation (2.12) - (2.13)).

2.3. Model validation

We set up two simulations to demonstrate the model's ability to replicate observations in both alluvial and mixed bedrock-alluvial conditions. These benchmark laboratory flume experiments documented: (1) the development of alternate bars in fully alluvial channels [Lanzoni, 2000a, b]; and (2) flow and sediment transport in mixed bedrock-alluvial channels [Chatanantavet and Parker, 2008]. Table 2.1 summarizes the conditions for each experiment.

2.3.1. Alternate bar formation in an alluvial channel

In the first experiment (Run P1505 [Lanzoni, 2000a, b]), a straight, flow- and sediment-recirculating flume 1.5 m wide, 1 m deep with a 55 m long test section was supplied with a steady water discharge of 30 l/s. The bed was composed of a uniform sand size of 0.48 mm and initially screeded flat. At the upstream end of the channel, a 16 m long, 5 m wide stilling basin was installed to ensure smooth and regular water and sediment discharge into the experimental channel. This experiment stopped as it reached equilibrium after 28 hours of a run when the water surface slope equated bed slope. A summary of reach-averaged measurements is reported in Table 2.1. Alternate bars were formed with an average height of 7 cm, wavelength of 10 m, and celerity of 2.80 m/h.

The simulation modeling Run P1505 is conducted with some modification of experimental conditions. First, a longer channel of 120 m was used to ensure the bar development to the

Table 2.1. Summary of experimental conditions. [a]

	m	m	%	l/s	g/s	mm	cm	m/s	hr
Run	B	L	S	Q_w	Q_c	D	H	U	t
P1505[b]	1.5	55	0.452	30	28	0.48	4.4	0.45	28
2-B2[c]	0.9	13	2	55	110	7	5.5	1.02	5

[a] B is the channel width, L is the channel length, S is the channel slope, Q_w is the water discharge, Q_c is the sediment transport capacity, D is the grain size, H is the averaged flow depth, U is the averaged flow velocity, and t is the duration of the experiment.
[b] Run P1505 was performed by Lanzoni [2000a, b].
[c] Run 2-B2 ($q_s/q_c = 0.56$) was performed by Chatanantavet and Parker [2008].

equilibrium state within the domain before leaving the channel reach [Defina, 2003]. Second, a small bump of 0.6 m long, 0.75 m wide, and 5 mm high was introduced near the upper boundary, left side (looking downstream), to create an initial disturbance to induce free bar development because the arbitrarily distributed source of disturbances from the physical experiment was unknown. Numerical models generally require perturbations such as a topographic bump [Defina, 2003; Wu et al., 2011] or a bend upstream of the straight channel [Mendoza et al., 2017] to develop bars in uniform flow over flat-bed conditions. Third, the constant and uniform water discharge and sediment feed rate were imposed at the inlet.

2.3.2. Patterns of bedrock alluviation with limited sediment supply

The second simulation Run 2-B2 ($q_s/q_c = 0.56$) [Chatanantavet and Parker, 2008], was carried out on a non-erodible bedrock surface in a 13 m long and 0.9 m wide straight, rectangular flume channel with a slope of 0.02. The bedrock bed was randomly abraded with a longitudinally averaged standard deviation of 2.4 mm, and the distance between the lowest and highest points of the profile is approximately 1 cm [Figure 1b and 3b, Chatanantavet and Parker, 2008].

The averaged values of initial experimental conditions are demonstrated in Table 2.1. The representative hydraulic roughness of the bedrock surface was back-calculated from the Manning-Strickler relation under the flow conditions measured from the experimental results conducted in the channel slope of 0.0115. Initially, the bed was covered entirely with a 2-cm-thick layer of uniform 7-mm sediment. The steady water discharge was 55 l/s, the constant sediment supply rate was 62 g/s, and the sediment transport capacity was estimated at 110 g/s for a wholly covered bed. The experiment stopped when the fraction of bedrock cover P_c reached a steady state whose value was approximately 0.59.

The numerical model simulation of this experiment uses a 0.9 m wide, 20 m long bedrock bed with randomly generated topographic perturbations with a standard deviation of 2.2 mm and a peak-to-peak distance of bed elevation of 0.9 cm (Figure 2.1). The roughness height due to skin friction (grain equivalent roughness height) used in the numerical simulation was back calculated from equation (2.4) using experimentally measured average flow conditions for each case of bare bedrock bed k_{sb} and alluvial bed k_{sa}. In the channel fully covered with sediment H = 0.06 m and U = 1.02 m/s, and in case of flow over bare bedrock bed H = 0.05 m and U = 1.22 m/s, hence k_{sa} = 7 mm and k_{sb} = 3 mm. The sediment supply to transport capacity ratio q_s/q_c is 0.6, which means the steady sediment supply rate is 66 g/s assuming the sediment transport capacity of the alluvial bed is 110 g/s. A small perturbation was given by changing sediment distribution patterns at the up-stream end of the channel to prevent sediment and bedform from washing out from the upstream end of the channel [e.g., Figure 14 in Inoue et al., 2016].

2.3.3. Simulations investigating impacts of roughness components on mixed bedrock-alluvial sediment dynamics

In order to explore the effect of roughness components on the model's performance of predicting alluvial patterns, we conducted numerical simulations without bedform roughness or ripple factor under the same conditions of Run 2-B2. The form drag effect on the flow is removed by setting the bedform roughness to zero; hence the ripple factor is no longer influential. The effect of bedform solely on sediment transport is removed by setting the ripple factor to unity.

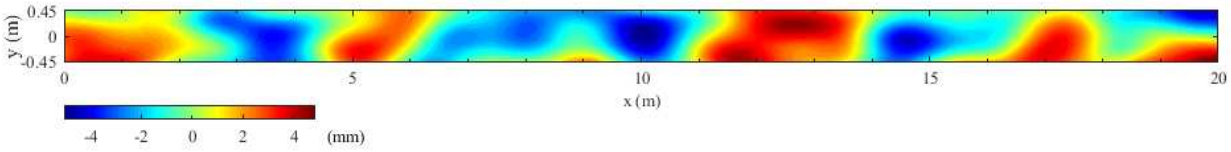

Figure 2.1. Plan view of bedrock topography. Colorbar scale indicates the detrended bed elevation.

We also conducted a simulation where the sediment transport roughness was set to zero, to explore how that component influences morphodynamic predictions in mixed bedrock-alluvial channels. For this simulation, the total roughness consisted of bedform and grain roughness, the latter of which was increased relative to the base scenario so that overall flow depths and velocities still matched experimental observations.

2.4. Results

2.4.1. Simulation of alluvial alternate bars (Run P1505)

Figure 2.2 shows the plan views of the evolution of detrended bed surface elevation in Run P1505. The initial upstream bump (t = 0 h) deflects flow and sediment transport. The sediment eroded from the bump forms the first bar and triggers the development of smaller bars downstream (t = 2 - 4 h). The bars migrate downstream as their size grows and lengthens, and pools deepen. When they reach equilibrium, their downstream migration and growth rate vary slowly and become stable. The initially flat alluvial bed, during the bedform formation and migration process, develops into a clear pattern of alternate bars. The initial disturbance gradually spreads out by decreasing height and stretching in the flow direction, prompting new bars to develop downstream [e.g., Figure 3 in Defina, 2003].

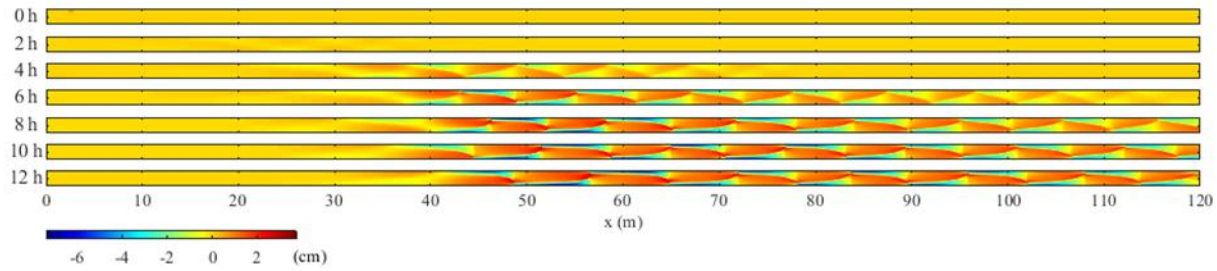

Figure 2.2. Detrended plan view of modeled bed evolution for the alluvial bar flume experiment (P1505) with the same longitudinal and transverse scale. Colorbar shows detrended bed elevation at the same scale for all plots.

The longitudinal bed profiles and the bed elevation difference between the right- and left-side walls from the numerical results (Figure 2.3) can be compared to the measured data at the equilibrium state from Lanzoni [2000a, Figure 1g] (Figure 2.4). Bar amplitudes are calculated as the difference between the right and left side of the bed elevation, measured 20 cm from each side wall (Figure 2.3a, b). The amplitude and wavelength are calculated using half the vertical and twice the horizontal peak-to-peak distances of the detrended profile. The celerity of migrating bars is calculated as the distance of the peaks from the different times divided by the time lag. The longitudinal bed profiles from numerical experiments exhibit highly-ordered wave patterns. The axis bed profiles in numerical simulation and experiment indicate the transversally maximum value of bed elevation.

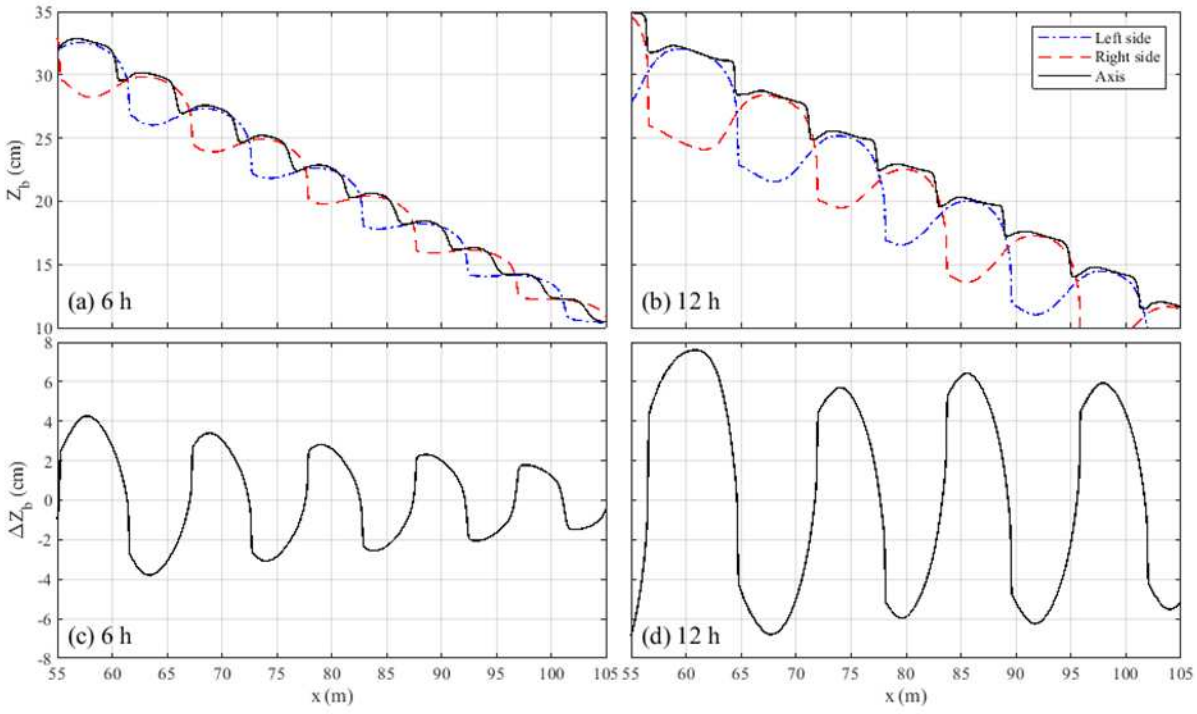

Figure 2.3. Modeled longitudinal bed profiles along the left- and right-side wall and axis at (a) 6 h and (b) 12 h and the difference between right- and left-side bed elevation at (c) 6 h and (d) 12h.

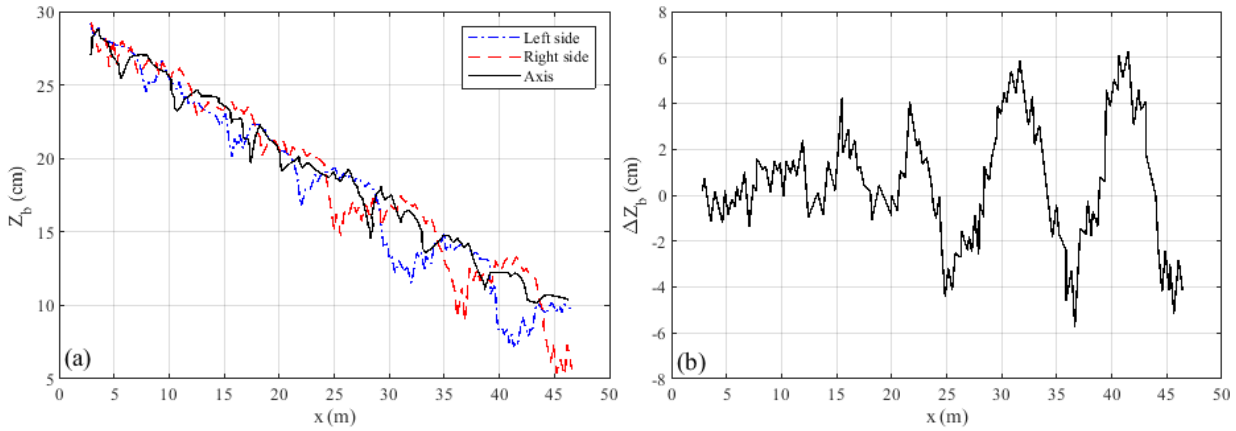

Figure 2.4. Measured (a) longitudinal bed profiles along the left- and right-side wall and (b) the difference between right- and left-side bed elevation at equilibrium [Figure 1g, Lanzoni (2000a)].

As the calculated time changes in bar celerity (Figure 2.5a, b), wavelength (Figure 2.5c, d), and amplitude (Figure 2.5e, f) are small, and we consider the bed condition at near equilibrium. The mean characteristics of the bar (bar height, wavelength, and celerity) near equilibrium are compared and reported in Table 2.2. The computed bar wavelength, height, and celerity are approximately 14 m, 7 cm, and 3.2 m/s, respectively. The computed bar height and celerity show reasonably good agreement with observations of Lanzoni [2000a], but the wavelength is slightly overestimated. However, the computed alternate bar wavelength is approximately nine times the channel width showing good agreement with Defina's [2003] numerical result and laboratory data of alternate bar wavelength prediction [Ikeda, 1984].

Table 2.2. Comparison of bar characteristics from measured data and computed results.

	m/h	m	cm
Run	C_b	λ_b	H_b
P1505	2.8	10	7
Computed	3.2±0.5	14±2	7±1

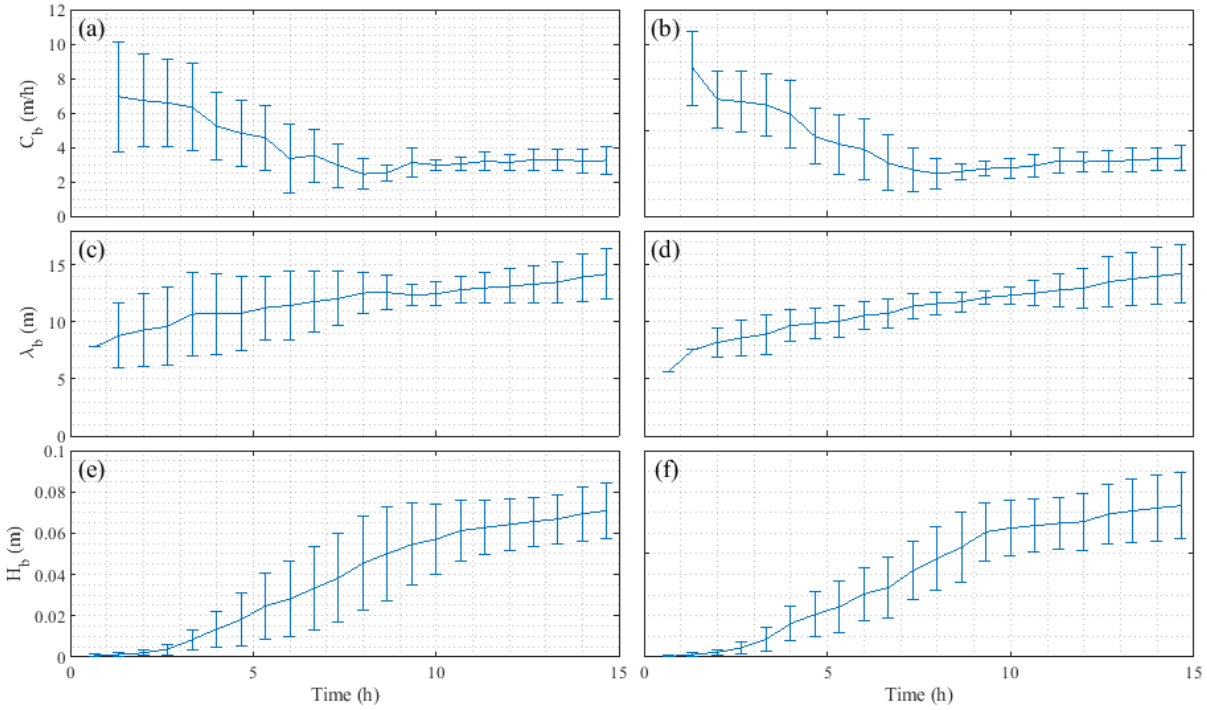

Figure 2.5. Computed time evolution of bar characteristics; celerity, wavelength, and amplitude (from top to bottom) on the left (a, c, and e) and right (b, d, and f) side of the channel.

2.4.2. Simulation of mixed bedrock-alluvial experiment (Run 2-B2)

Figure 2.6 shows a series of numerical results illustrating the time evolution bed configuration for the mixed bedrock-alluvial experiment (Run 2-B2) commencing from a 2 cm thick alluvial cover (t = 0 h). The non-uniform sediment distribution, feeding more sediment at one side than the other, causes flow deflection induced by a laterally sloping bed at the upstream end (t = 0.5 h). At an early stage, this disturbance quickly erodes sediment on the right side of the channel down to the bedrock bed and creates pools and bars downstream. Then the exposed bedrock bed area, indicated as a white area, increases as the pools deepen and bars grow taller (t = 1 h). The sediment on the bed forms a strip of sediment shifting from one side to the other side of the channel through time while maintaining the area fraction of bedrock cover. Similar patterns were observed in the Chatanantavet and Parker [2008] experiments; for example, Figure 2.7 shows the time

evolution of bedrock exposure from Run 2-B4 [Table 1 in Chatanantavet and Parker, 2008] with $Q_s = 97$ g/s, $q_s/q_c = 0.88$, and $P_c = 0.78$ at equilibrium phase. Again, a continuous band of sediment forms comparable to Figure 2.6. However, the sediment cover is more expansive, and the bed sediment shifting from one to the other side is less sensitive because of the higher sediment supply rate than what was provided in Run 2-B2 modeled here.

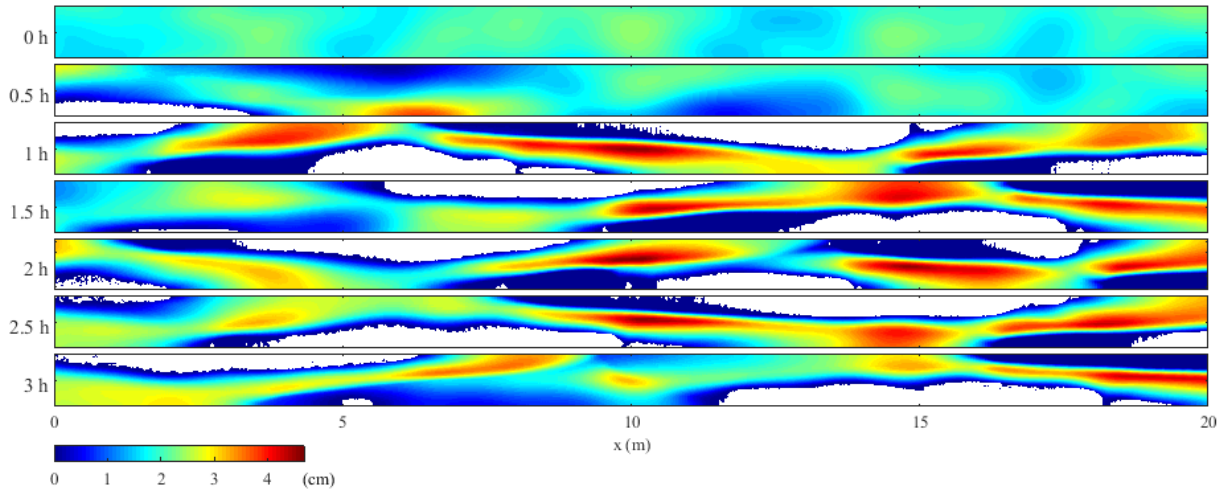

Figure 2.6. Simulated bed evolution of Run 2-B2. Colorbar shows the thickness of the sediment cover, and white areas correspond to the exposed bedrock surface.

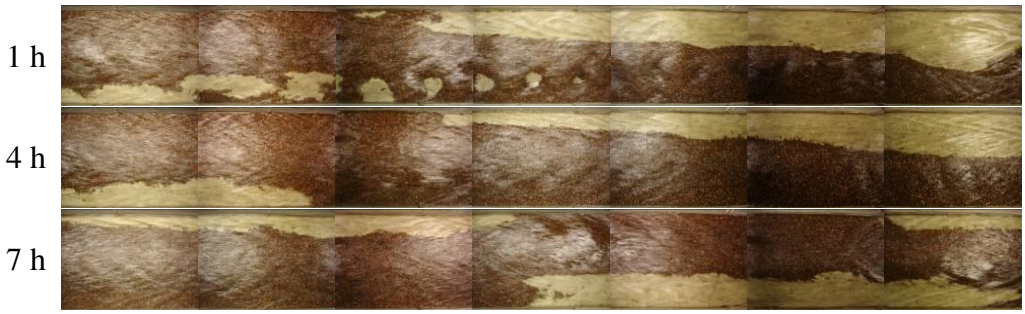

Figure 2.7. Time evolution of bedrock exposure Run 2-B4: $Q_s = 97$ g/s, $q_s/q_c = 0.88$, and $P_c = 0.78$ [Chatanantavet and Parker, 2008 (personal communication)]. The channel is 0.9 m wide, 13 m long, water and sediment flow from left to right, and light and dark areas correspond to bedrock and sediment, respectively.

Figure 2.8 shows the computed flow variables, bed topography, and sediment transport capacity at equilibrium (t = 5h). The flow depth and velocity over the exposed bedrock area are higher than on the alluvial bed. However, calculated shear stress is lower in exposed bedrock areas due to the smaller roughness and higher flow depth. The critical dimensionless shear stress is generally higher on the alluvial bed but smaller over the lee side of the bedforms. The sediment transport capacity tends to be higher over the exposed bedrock surface and stoss side of the bedform and lower on lee slopes.

Figure 2.9 shows the time evolution of channel averaged fraction of bedrock exposure F_e = 1 - P_c, alluvial thickness, relative Shields parameter, and bed load transport rate. A ratio of alluvial coverage of bed surface in the area of interest determines the fraction of bedrock covered with sediment $P_c = A_c \,/\, A_t$ [Johnson, 2014], where A_c is the area covered with sediment and A_t is the total area of interest, or numerically $P_c = \sum P_{ci} \,/\, N$, where P_{ci} is the local fraction of bedrock cover (equation 2.8) and N is the total number of cells in the domain. The fraction of bedrock exposure is initially zero when the bed is entirely covered by sediment and quickly converges toward a near-equilibrium state where F_e is 0.4 at t = 1 h (Figure 2.9a). The numerical result of the degree of bedrock exposure presents a similar value of F_e to the experimental observation. The averaged sediment cover thickness over an alluvial area varies little in the range of the length of one grain sizes (Figure 2.9b). The relative Shields parameter τ^*/τ_c^* (Figure 2.9c) and bed load transport rate (Figure 2.9d) decrease from an initially higher value to approximate equilibrium and vary around 1.2 and 70 g/s, respectively.

The comparison between the computed and measured quantities available from experimental observations is presented in Table 2.3. The agreement is reasonably good in predicting the fraction of bedrock cover, but higher flow depth and lower velocity in the experiment result in a

lower Froude number and lower dimensionless shear stress. The model predicted less shear stress over the bare bedrock areas than the alluvial areas because the bedform developed during the simulation. The alluvial bars form where flow depth is low and velocity is high, and pools exist over the bare bedrock area with deep flow depth and low velocity.

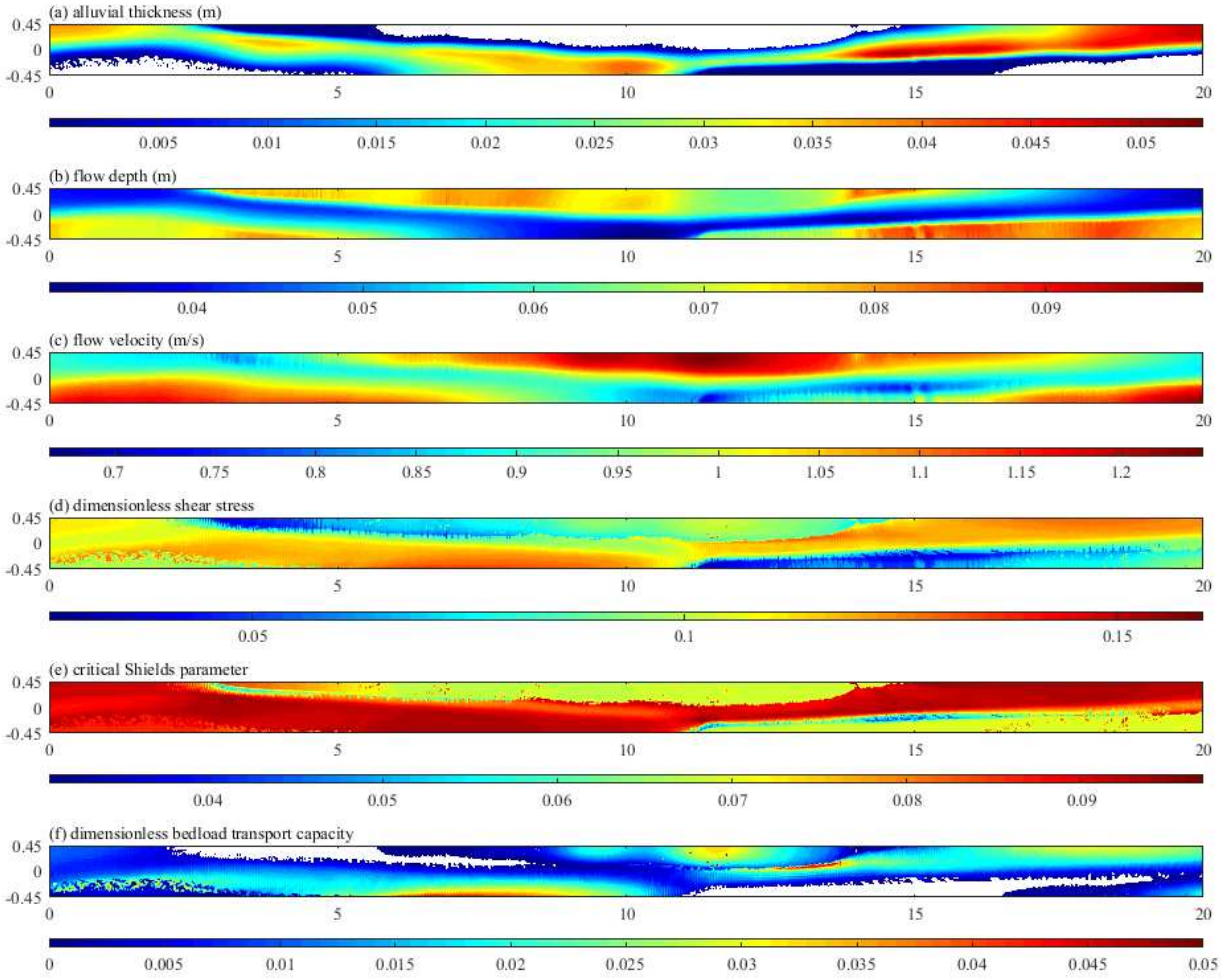

Figure 2.8. Plan view of (a) alluvial thickness, (b) flow depth. (c) flow velocity, (d) dimensionless shear stress, (e) critical Shields parameter, and (f) dimensionless bed load transport capacity at t = 5 h. Colorbars indicate the scale of computed values, respectively, and white areas correspond to (a) the exposed bedrock surface and (e) zero sediment transport rate.

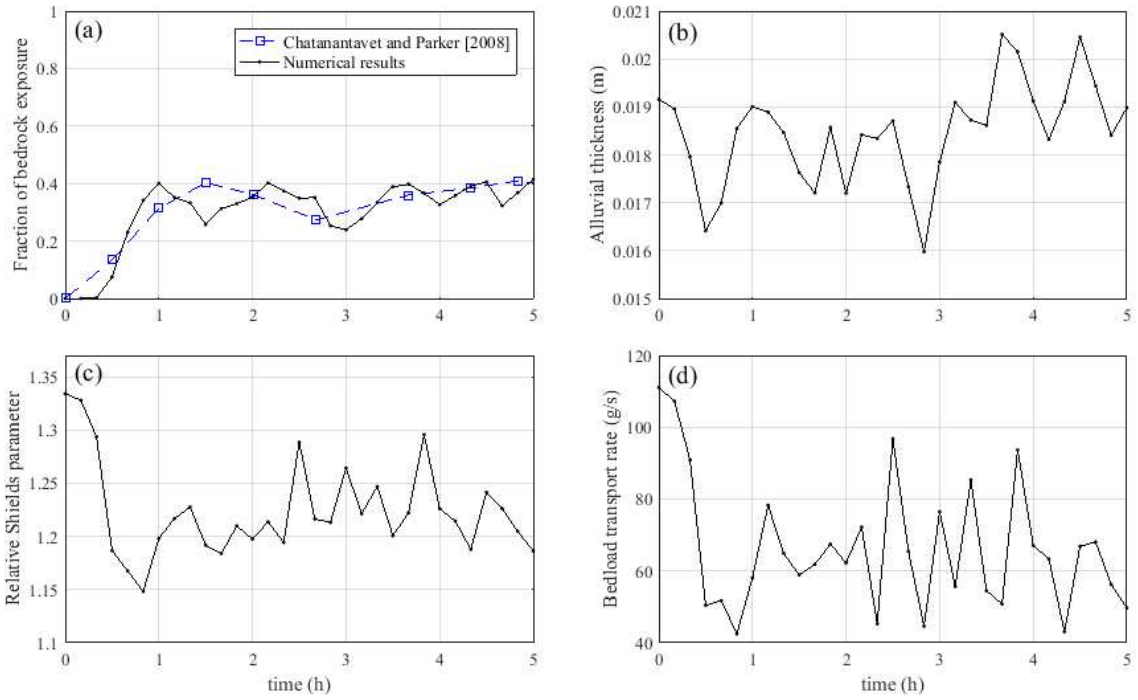

Figure 2.9. The time evolution of the (a) fraction of bedrock exposure from numerical and experimental results, (b) averaged alluvial thickness over the part of the bed covered with sediment, (c) relative Shields parameter, and(d) sediment transport rate.

Table 2.3. Summary of numerical results

		cm	m/s		
Run	P_c	H	U	Fr	τ^*
2-B2 [C&P][a]	0.59	5.5±1.5	1.11	1.51	0.11
2-B2[b]	0.60	6.0	1.00	1.32	0.10
2-B2 (covered zones) [c]		5.6	0.95	1.31	0.10
2-B2 (exposed zones) [d]		7.5	1.07	1.26	0.08

[a] Experimental results from Chatanantavet and Parker [2008].
[b] Reach averaged numerical results.
[c] Reach averaged numerical results only over the alluviated zones.
[d] Reach averaged numerical results only over the exposed bedrock zones.

2.5. Discussion

The present study shows the results that bed topography comparable to experimental observations from (1) free bar formation in a mild slope alluvial channel with fine grains [Lanzoni, 2000a] and; (2) alluvial pattern in the mixed bedrock-alluvial channel in a steep slope channel with coarse grains [Chatanantavet and Parker, 2008]. These suggest that the model can simulate complex flow and sediment transport to gain insight into mechanisms of the bedform development and alluviation patterns in mixed bedrock-alluvial channels.

The discrepancies between the numerical and experimental results are mainly associated with the initial and boundary conditions, which are not successfully reflected in the numerical models, such as the size of the initial disturbances and patterns of flow and sediment distribution at the channel inlet. In addition, the empirical parameters assumed and employed in the numerical model lead to an inability to predict bed evolution accurately.

2.5.1. Discussion on ripple factor and form drag

Only a few studies have attempted to simulate sediment transport in a straight mixed bedrock-alluvial channel using a 2D numerical model [Nelson and Seminara, 2012; Inoue et al., 2016]. These models estimated bed resistance to the flow using the grain roughness and bedrock surface irregularity which is applicable to the plane bed. Our model includes the effect of bedform generation in roughness estimation since alternate bars often form in mixed bedrock-alluvial channels [Chatanantavet and Parker, 2008; Nelson and Seminara, 2012; Inoue et al., 2016]. The hydraulic roughness height of alluvial bed changes according to the size of bedforms (i.e., dunes and ripples) [Vanoui and Hwang, 1967; Engelund, 1977; Van Rijn, 1982, 1984; Wiberg and Nelson, 1992; Raudkivi, 1997].

Figure 2.10 shows the time evolution of bed topography with the same condition applied in Run 2-B2 without including the bedform effect in the roughness calculation, and hence the ineffective ripple factor. This simulation undergoes sediment washing out from the upstream end of the channel while forming a bar-like bedform downstream. This result is comparable with the results provided by Inoue et al. [Figure 14, 2016].

The prediction of bed load transport is based on the corrected dimensionless shear stress for bedform roughness with a ripple factor [Meyer-Peter and Mueller, 1948]. The value of the ripple factor has not been reported explicitly but empirically estimated as a ratio of grain shear stress to the total bed shear stress [Vermeer, 1986; Ribberink, 1987]. Nevertheless, the ripple factor is often applied to sediment transport models to generate bedforms in alluvial channels with a constant value of less than 1 [Defina, 2003; Van der Meer et al., 2011].

Figure 2.11 shows the plan view of the bed topography of Run 2-B2 without the dimensionless shear stress correction by using a ripple factor equal to 1 in equation (2.16). The upstream sediment erodes slower than the bed evolution in Figure 2.10, and the morphodynamic process has enough time to form a longitudinal sediment strip because the form drag generates higher flow resistance. However, larger dimensionless shear stress due to the absence of the ripple factor in the supply-limited channel causes a thin layer of sediment at the upstream end and a narrow strip of sediment. The strip of sediment is cut off at the narrowed section, and the sediment is eventually washed out.

Comparing Figures 2.6 and 2.10-11, it can be seen that introducing both form drag to the roughness and ripple factor of the shear stress in bed load transport is critical in developing bedforms and persistent alluviation in bedrock channels where the sediment supply is less than the capacity of the channel. Results from previous models attempting to replicate these experiments

[Inoue et al., 2014] show alternate bar development over the alluvial surface, but sediment supply less than the transport capacity decreases the thickness of the alluvial layer leading to sediment washing out from upstream and exposure of the entire bedrock.

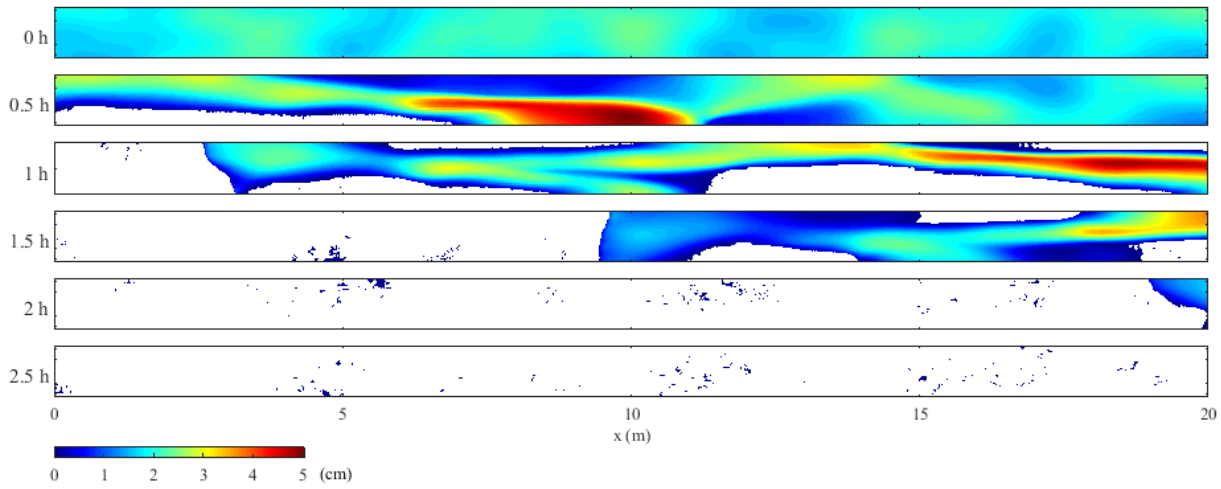

Figure 2.10. The time evolution of bed exposure for run 2-B2 without form drag effect ($k_f = 0$). Colorbar means alluvial cover thickness, and white area is exposed bedrock surface.

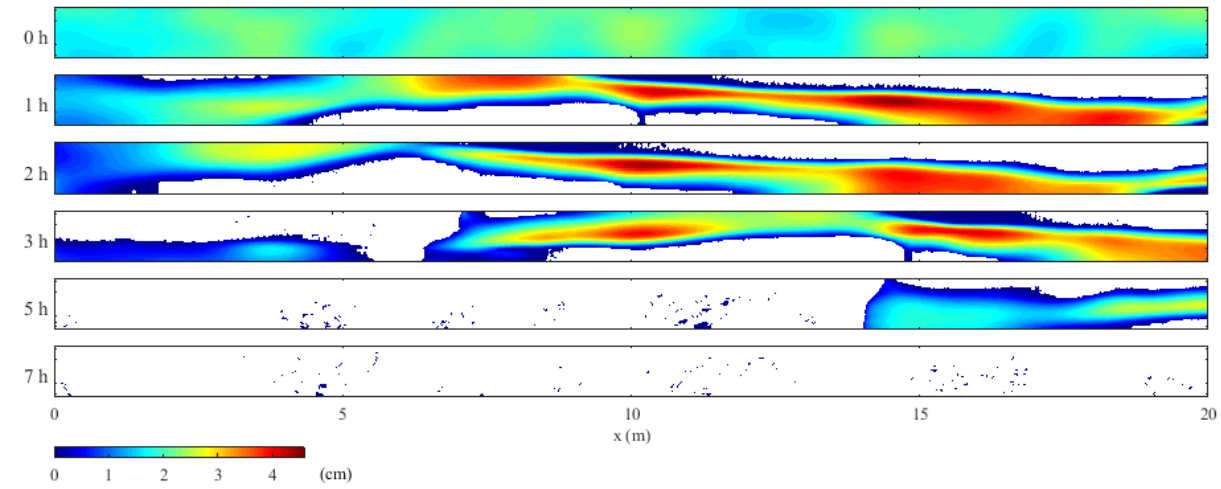

Figure 2.11. The time evolution of bed exposure for Run 2-B2 without ripple factor ($\mu = 1$). Color-bar indicates alluvial cover thickness, and the white area is exposed to the bedrock surface.

The roughness component for form drag effectively increases drag and reduces flow velocity, whereas the ripple factor reduces shear stress in bedform-developed areas. Unlike the form drag acting on entire bedform fields, skin friction is responsible for the local bed surface roughness only. The smaller surface roughness over the exposed bedrock area than over the alluvial area produces higher shear stress. Therefore the model absent of form drag and ripple factor predicts a higher sediment transport rate as the fraction of sediment cover decreases in limited sediment supply conditions result in a total washout of the sediment from the channel.

2.5.2. The impact of sediment transport roughness

Our model explicitly accounts for both the grain roughness and roughness produced by moving particles [Smith and McLean, 1977; Grant and Madsen, 1982; Dietrich, 1982; Wiberg and Rubin, 1989]. To explore the importance of accounting for each of these components individually, we conducted a simulation where we ignored sediment transport roughness and increased the grain roughness to compensate for reduced bed roughness caused by the absence of sediment transport roughness.

Figure 2.12 shows the time evolution of bed topography for this simulation of Run 2-B2, excluding sediment transport roughness. A strip of sediment forms shifting from one side to the other side of the channel momentarily (t = 0.5 h), but then washes out from the upstream end of the channel (t = 2 h), with a small residual alluvial patch persisting only in a topographic low area in the bedrock (t = 4 h). The flow resistance decreases as bedrock gets exposed because of the underlying linear relationship between the fraction of bedrock cover and grain roughness. Unlike grain roughness, the sediment transport roughness is larger where grain movements actively take place. The sediment transport roughness tends to be higher over the bedrock surface partially

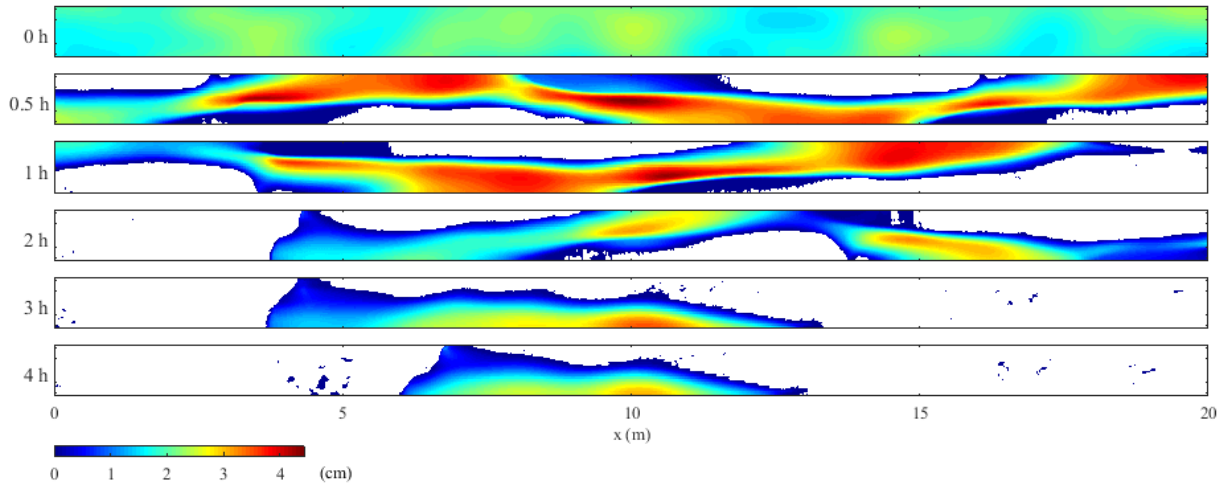

Figure 2.12. The time evolution of bed exposure for Run 2-B2 without sediment transport roughness from flow resistance ($k_t = 0$). Colorbar indicates alluvial cover thickness, and the white area is exposed to the bedrock surface.

covered with sediment because the sediment transport rate over the smoother bedrock surface, where the flow velocity is faster, is higher than over the rougher alluvial surface. The sediment transport roughness contributes to the formation of alluvial patches in the bedrock channel by reducing grain entrainment over the mixed bedrock-alluvial surface. These results indicate that separate accounting of grain and sediment transport roughness produces morphodynamic predictions that better match observations of persistent alluvial patterns in mixed bedrock-alluvial channels.

2.6. Conclusions

In this study, we have developed a two-dimensional morphodynamic model to explore bar formation and migration in an alluvial channel and sediment transport mechanisms in a mixed bedrock-alluvial channel without sufficient sediment supply. Comparisons of model predictions with experimental observations from the free bar test show that the model predicts bed morphology and bedform development similar to the observations of the flume experiment. However, some discrepancies raise the need for proper tuning of model parameters and initial bottom perturbation.

The model predicts the flow field and sediment distribution patterns in mixed bedrock alluvial channels reasonably well. Numerical experiments show that the inclusion of bedform roughness and a shear stress correction for near-bed sediment transport is critical to be able to replicate the alluvial patterns over bare bedrock observed in flume experiments. The evolving interactions between the alluvial and bedrock bed surface, flow field, and sediment transport simultaneously modify the degree of sediment cover and bed topography. The numerical model presented in this study captures the behavior associated with the bedrock alluviation process and can be used to extend its applicability to various flow and sediment supply conditions with different channel slopes and antecedent topography.

Future work could explore the mechanisms of sediment pattern formation in mixed bedrock-alluvial rivers and characterize the effects of the channel slope, initial sediment cover thickness, difference between the grain and bedrock roughness, and bedrock configuration.

CHAPTER 3

CONTROLS ON PATTERNS OF ALLUVIATION IN MIXED BEDROCK-ALLUVIAL CHANNELS

3.1. Introduction

Bedrock channels are characterized by occasional or continuous exposures of nonalluviated bedrock, which is a consequence of these channels receiving a sediment supply that is less than their transport capacity. A wide variety of models for drainage network evolution distinguish between bedrock and alluvial reaches [Howard, 1980; Howard and Kerby, 1983; Howard et al., 1994; Montgomery et al., 1996] by using channel slope and discharge to express channel transport capacity. Field investigations [Montgomery et al., 1996; Montgomery and Buffington, 1997; Massong and Montgomery, 2000; Lamb et al., 2008] demonstrate that bedrock channels occur at slopes greater than a critical value ($S > S_c$), and alluvial channels form at a slope less than the critical value ($S <= S_c$).

The spatial distribution of alluvial cover in mixed bedrock-alluvial channels has importance for determining rates and patterns of bedrock erosion, hydrodynamics, and aquatic habitat. Mechanistic models of bedrock erosion incorporate the erosional mechanism of saltating bed load particles impacting and eroding bedrock [e.g., Sklar and Dietrich, 1998, 2001, 2004; Hartshorn et al., 2002; Demeter et al., 2005; Zhang et al., 2015], implicitly introducing dependence on sediment supply and bedrock exposure into the calculation of erosion rates. Competition between the tools and cover effects controls the spatial distribution of the bedrock channel erosion, resulting in lateral and vertical channel erosion and meandering [Finnegan et al., 2007; Turowski et al., 2007, 2008a, b; Lamb et al., 2015]. The cover effect is typically demonstrated by linear or

exponential relations of fractional bedrock exposure as a function of sediment supply to transport capacity ratio [Sklar and Dietrich, 1998, 2004; Turowski et al., 2007]. Additionally, sediment supply and alluvial cover impact the maintenance and distribution of aquatic habitat and attached micro-organisms [Lisle and Hilton, 1992; Lisle and Lewis, 1992; Madej, 2001; Buffington et al., 2004; Detert and Parker, 2010; Kuhnle et al., 2013; Huston and Fox, 2015, 2016].

Alluvial patterns in bedrock channels are controlled by spatial and temporal variations in sediment flux, transport capacity, and bed topography. These channels can exhibit alluvial patterns ranging from continuous and concentrated longitudinal strips of sediment to spatially discontinuous patches of sediment. Experiments in mixed bedrock-alluvial channels have observed spatially concentrated sediment cover and storage in low parts of the underlying bedrock topography [Finnegan et al., 2007; Johnson and Whipple, 2007], indicating that topographic roughness induces changes in local flow properties and threshold of sediment motion. Inoue et al. [2014] observed inconsistent development of alluvial cover in the inner channel through their field experiments. Hodge and Hoey's [2016a, b] experiments show that velocity is an important control on sediment deposition, as they did not observe sediment cover at low areas of the bed where the flow velocity remained high. The results from several experimental studies [Sklar and Dietrich, 2004; Turowski et al., 2007; Chatanantavet and Parker, 2008; Johnson and Whipple, 2010] suggest a few major factors control grain entrainment and bedrock exposure, such as sediment supply rate, channel slope, material size, and bed roughness.

A set of flume experiments [Chatanantavet and Parker, 2008] using different channel bed slopes has shown that for lower slopes ($S < 0.0115$) bedrock exposure decreased more or less linearly with increasing the ratio of sediment supply rate to capacity transport rate. However, for sufficiently higher slopes ($S \geq 0.0115$), the bedrock remained fully exposed when the ratio of

sediment supply to transport capacity is less than a critical value, while a linear relationship between the degree of bedrock exposure and sediment supply rate to transport capacity ratio prevailed when the sediment supply exceeds transport capacity. These experiments also documented a slope-dependent "runaway alluviation," where for initially bare-bedrock conditions, low-slope channels develop linearly increasing sediment cover with increasing sediment supply, while high-slope channels remain completely exposed until sediment supply exceeds the transport capacity, beyond which the channel becomes fully alluviated. Chatanantavet and Parker [2008] suggested this may be a result of slope-dependent grain interactions; later experiments by Mishra and Inoue [2020] indicated that runaway alluviation occurred when the bedrock roughness was lower than the sediment roughness, but the gradual alluvial cover could develop when the bedrock roughness was higher than that of the sediment. A full explanation of the slope-dependent behavior of sediment dynamics in mixed bedrock-alluvial channels is still needed.

Morphodynamic models have struggled to replicate the types of observations made in mixed bedrock-alluvial experiments. Promising results have been presented by Hodge and Hoey [2012], who developed a cellular automaton (CA) model where the probability of entrainment of individual grains was specified for bedrock or alluvial areas. Their model found relationships between bedrock exposure and the ratio of sediment supply to transport capacity (q_s/q_c) similar to those observed by Chatanantavet and Parker [2008], but in contrast to the experimental observations, the majority of their CA model runs predicted that the presence or absence of sediment cover on the bed at the beginning of the run did not affect the steady state sediment cover. Additionally, the entrainment probabilities needed to change from run to run for their results to achieve the diversity of findings Chatanantavet and Parker [2008] reported. While CA models like this provide interesting insight on the potential importance of grain dynamics for alluvial patterns in bedrock-

alluvial channels, the absence of a flow model makes connecting probabilities of sediment entrainment and deposition to physical mechanisms of sediment transport and alluviation challenging.

Because of the complexity inherent in the roughness relationship incorporated to the flow resistance and sediment transport, evaluating the relative influence of different roughness mechanisms for channel evolution is currently a challenging problem. The patterns of sediment cover over the bedrock bed affect the spatial distribution of local roughness, flow rate, and sediment transport. Here we use a new morphodynamic model to reproduce many of the phenomena that have been observed in mixed bedrock-alluvial channels, and we use the model predictions to untangle the mechanisms responsible for the range of dynamic sediment behavior in these environments. In particular, we use the model to investigate the following questions: 1) what explains the apparent slope dependence for runaway alluviation? 2) How can mixed bedrock-alluvial channels maintain alluvial cover when the sediment supply is less than the transport capacity? 3) How do initial conditions of sediment cover affect the temporal development of alluvial cover, and the overall relationship between bedrock exposure and sediment supply? Our results reveal the important interactions between dynamic channel roughness, flow patterns, sediment transport rates, bedform development, and alluvial cover.

3.2. Methods

3.2.1. Morphodynamic model

We have developed a two-dimensional numerical morphodynamic model for mixed bedrock-alluvial channels. The model consists of three major components: (1) the 2D shallow water equations (SWE) in the depth-averaged form are applied to solve the hydrodynamical component, (2) a sediment transport model calculates bed load transport rates associated with the

hydrodynamic variables and topographic variation, and (3) the modified Exner equation is appropriately adopted to bed level changes due to the sediment transport processes. The novel aspects of this model, compared to previous models applied to mixed bedrock-alluvial morphodynamics, are 1) the Exner equation of sediment continuity accounts for the volume of bed load in transport and the fraction of bed covered in sediment, 2) a composite alluvial and bedrock roughness is used in the flow calculation, 3) the friction for sediment transport is modified to account for the effects of bedforms, and 4) the numerical scheme is robust and capable of handling Froude transitions and capturing shocks. We summarize the key components of the model below, but a complete description can be found in Chapter 2.2.

A key assumption in most numerical models combining water flow, sediment transport, and morphological evolution is that the response time of bed evolution is relatively long compared to the timescales of relevance to the flow of water [McLean et al., 1994; Tubino et al., 1999; Nelson et al., 2003]. This allows a decoupling between the water flow computation and the sediment equation by assuming a quasi-steady approximation of morphodynamic process that the bed level does not change rapidly during an infinitesimal time interval while the flow field adapts instantaneously. Thus, the decoupled model practically solves for the flow field and topographic evolution using an iterative procedure.

The numerical model regarding hydro- and morphodynamic processes in mixed bedrock-alluvial channels must deal with the roughness difference between alluvium and bedrock surface and the effect of form drag of bedforms on the flow resistance and bed shear stress for sediment transport predictions. To account for this, we adopt composite roughness partitioned into surface roughness of alluvial and bedrock bed, sediment transport roughness, and form drag. The ripple

factor is applied to the shear stress to remove the form drag of the bedforms assuming the remaining part is responsible for sediment transport.

The water flow depth and flux are calculated using the weighted average flux (WAF) discretization with Harten-Lax-van Leer-Contract (HLLC) solver [Toro, 1992a, b] and an explicit application of the central difference of the viscous and friction terms at each computational cell center in a 2D domain. Because of the local and global change in flow resistance associated with different substrate roughness between the bedrock and bed material and bedform evolution, a treatment of transcritical flow is necessary. The flow resistance consists of skin friction, form drag, and bed load transport roughness. The linear cover fraction model representing the relation between the alluvial bed and bare bedrock bed, the volume of local bed material per volume of a monolayer of sediment grains, is used to calculate local skin friction. The form drag effect is determined using the local bed slope and topographic variation averaged over the area of interest. Additionally, the bed load layer thickness is added to the total roughness where the sediment transport occurs. In Chapter 2.2.3, we demonstrated that explicit calculation of each of these components of roughness was critical to be able to replicate observations of persistent sediment cover in mixed bedrock-alluvial channels.

The bed morphology is updated using the modified Exner equation for sediment continuity [Luu et al., 2004; Inoue et al., 2014, 2016]. The sediment transport capacity on the alluvial bed is estimated from Wong et al. [2007]. A correction of the bed load transport rate on the pure bedrock bed is necessary considering a relatively small volume of bed load transport (equation 2.19). When the bed is completely bare, only the volume of sediment in the bed load layer is brought into bed load transport without resting on the bed, referred to as the throughput bed load. When the volume of the bed load layer exceeds the saturation value, sediment starts to deposit on the bed and the

linear cover fraction model is utilized to determine whether the bed is in the state of partial or complete cover (equations 2.12-2.14).

The skin friction is used for the calculation of dimensionless shear stress to account for the fact that only the near-bed grain roughness is responsible for the sediment transport, using a correction referred as to the ripple factor [Vermeer, 1986; Ribberink, 1987]. The dimensionless shear stress [Struiksma, 1985; Talmon et al., 1995] and critical Shields number [Soulsby, 1997; Calantoni, 2002; Duan and Julien, 2005] are corrected for spatially varying bed topography in the direction of flow.

The critical Shields parameter calculated as a function of the ratio of the bedrock hydraulic roughness to the grain size [Inoue et al., 2014; Johnson, 2014; Mishra et al., 2020] is adopted instead of constant value for bedrock and alluvial surfaces. We use a modified dimensionless critical shear stress model (equation 3.1) to simulate bed evolution in different channel slopes:

$$\tau_c^* = \alpha_c (k_0/d)^{0.6}\,, \tag{3.31}$$

where α_c is the correction factor for different channel slope, k_0 is the hydraulic roughness height, and d is the grain size.

3.2.2. Simulation conditions

We conducted a set of numerical experiments to explore how patterns of alluvial cover in a mixed bedrock-alluvial channel evolve for different channel slopes, initial cover thicknesses, and varying sediment supply rates. The simulations were designed to complement the experiments of Chatanantavet and Parker [2008] and provide mechanistic insight into controls on alluvial patterns in bedrock channels. Table 3.1 summarizes the initial flow and sediment condition used in each experiment based on the flume experiments conducted by Chatanantavet and Parker [2008]. The

computational channel is straight and longer than the experimental channel to avoid possible problems regarding bedform development sensitive to boundary disturbances. This study focuses on the morphodynamic mechanisms responsible for sediment cover patterns and bed evolution. We adopt simplified analysis conditions such as the constant influx of water and sediment at the upstream boundary, uniform sediment size, and non-erodible bedrock to exclude potential disturbances to bed topography created by unsteady conditions. The computations are stopped when near equilibrium conditions of bed topography are achieved, in which the average sediment cover thickness and the fraction of bedrock cover vary around stable values.

Table 3.1. Summary of flow, sediment transport, and topographic conditions

	mm		%	cm	l/s	g/s	g/s		mm	cm	cm/s	
RUN	k_b	α_c	S	Z_{bi}	Q_w	Q_c	Q_s	Q_s/Q_c	d	H	U	F_e
2-A1	0.4	0.03	1.15	1.5	24	25	5	0.2	2	4.3	62	0.78
2-A2	0.4	0.03	1.15	1.5	24	25	10	0.4	2	4.3	62	0.6
2-A3	0.4	0.03	1.15	1.5	24	25	15	0.6	2	4.3	62	0.41
2-A4	0.4	0.03	1.15	1.5	24	25	20	0.8	2	4.3	62	0.27
2-A5	0.4	0.03	1.15	1.5	24	25	25	1.0	2	4.5	59	0
2-B1	4	0.05	2	2	55	110	44	0.4	7	5	122	1
2-B2	4	0.05	2	2	55	110	66	0.6	7	5.5	111	0.4
2-B3	4	0.05	2	2	55	110	88	0.8	7	5.5	111	0.25
2-B4	4	0.05	2	2	55	110	110	1.0	7	6	102	0
2-B2-a	4	0.05	2	1	55	110	66	0.6	7	5	122	1
2-B2-b	4	0.05	2	4	55	110	66	0.6	7	6	102	0.4
2-B2-c	4	0.05	2	6	55	110	66	0.6	7	6	102	0.4
2-Ax	0.4	0.03	1.15	0	24	150	150	1.0	2	2.9	92	0
2-Bx	4	0.05	2	0	55	350	350	1.0	7	5	122	0
2-Dx-a	0.2	0.08	0.3	0	55	8	2	0.25	2	7.5	81	0.7
2-Dx-b	0.2	0.08	0.3	0	55	8	4	0.5	2	7.5	81	0.6
2-Dx-c	0.2	0.08	0.3	0	55	8	6	0.75	2	7.5	81	0.52
2-Dx-d	0.2	0.08	0.3	0	55	8	8	1.0	2	7.5	81	0

The run names correspond to Chatanantavet and Parker's [2008] experimental conditions. k_b denotes bedrock roughness height, α_c denotes Shields number correction coefficient, S denotes channel slope, Z_{bi} denotes initial sediment cover thickness, Q_w denotes water discharge, Q_c denotes sediment transport capacity, Q_s denotes sediment supply rate, q_s/q_c denotes the ratio of sediment supply to transport capacity, d denotes grain size, H denotes flow depth, U denotes flow velocity, and F_e denotes the fraction of bedrock exposure, respectively.

All simulations are performed in a planar bedrock bed channel having a length of 20 m and a width of 0.9 m. A small perturbation of topographic variation with a standard deviation of 2.2 mm and peak-to-peak bed elevation of 9 mm is applied to the bedrock bed. Various hydraulic conditions are considered, for example, a broad range of sediment supply, bed slope, hydraulic roughness of bed surface, and antecedent alluvial layer thickness. First, two sets of simulations are performed: (1) with some initial cover thickness with different channel slopes (Runs 2-A5 and 2-B5) and (2) without antecedent sediment cover (Runs 2-Ax, 2-Bx, and 2-Dx) to explore the effect of channel slopes. Second, a set of Run 2-B is conducted with the $q_s/q_c = 0.6$ and various initial sediment cover thicknesses of 1, 4, and 6 cm. Two types of uniform grains, fine 2 mm and coarse 7 mm gravels, are employed in the experiments with mild slope channel ($S \leq 0.0115$) and with steep slope channel ($S = 0.02$), respectively.

The bedrock and grain roughness heights are back-calculated from the logarithmic law depending on the channel slope and corresponding hydraulic conditions. The spatially varying friction coefficient is then calculated as a function of the flow depth and composite roughness, which depends upon the local status of fraction cover, bedform dimension, and bed load transport rate. The critical Shields parameters for each channel slope are back-calculated by equating the sediment transport capacity from our numerical simulations and experimental runs of Chatanantavet and Parker [2008] conducted in bedrock channels, and adjustment to the correction coefficient α_c is employed.

In each simulation, the sediment supply q_s was specified as a target fraction of the transport capacity q_c. To determine q_c, we conducted simulations for each run, assuming that the initial bed is nearly flat for either with initial sediment cover (Runs 2-A and 2-B) or bare bedrock surface (Runs 2-Ax, 2-Bx, and 2-Dx) without the presence of bedforms. The bedrock transport capacity is

the amount of sediment input per unit width fed into the initially bare bedrock bed equivalent when the channel bed is thoroughly covered with sediment. The alluvial transport capacity is the channel averaged sediment transport rate in the alluvial channel.

3.3. Results

3.3.1. Simulations with no initial alluvial cover

Runs 2-Ax, 2-Bx, and 2-Dx all commenced with a bare bedrock bed, and are used to investigate how channel slope affects sudden vs. gradual alluviation as sediment supply increases. The lowest-slope simulations (S = 0.003) of Run 2-Dx exhibited a gradual decrease in bedrock exposure at increasing sediment supplies. An example of bed evolution for these runs is shown in Figure 3.1 for Run 2-Dx-a. The initial flow depth of 7 cm and constant water flux of 55 l/s over a bare bedrock bed calculate 0.2 mm of bedrock surface roughness. The amount of sediment flux with a uniform grain size of 2 mm constantly supplied into the channel at the inlet is 2 g/s corresponding q_s/q_c = 0.25. The time evolution of bed topography illustrates that the sediment grains start to settle and scatter in the lower topography areas than their surroundings. The extent of sediment patches gradually grows thicker and expands toward the upstream direction.

Figure 3.2 shows the final state of alluviation for all of the low-slope 2-Dx runs. As sediment supply (i.e., q_s/q_c) increases, the alluviated patches grow in size and the overall fraction of exposed bedrock (F_e) decreases.

Figure 3.3 shows the time evolution of the alluvial patch formation for the simulation of Run 2-Bx commenced from the bare bedrock bed in a channel with a slope of 0.02. The initial flow depth of 5 cm and constant water flux of 55 l/s over a bare bedrock bed calculate 4 mm of bedrock surface roughness. A uniform 7 mm sediment is supplied into the channel at the upstream

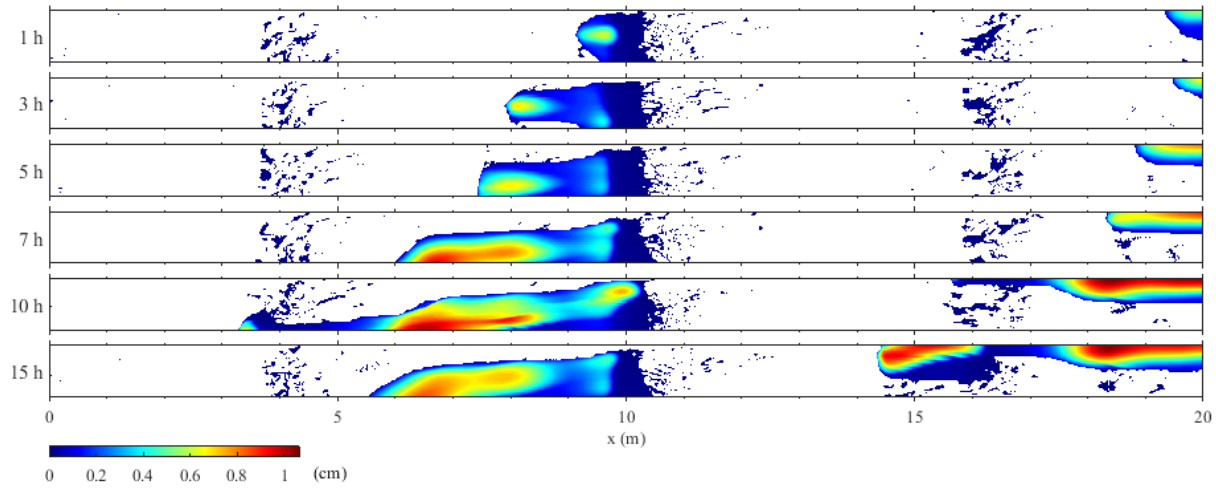

Figure 3.1. Simulated bed evolution of Run 2-Dx-a, which began with a bare bedrock bed and sediment supplied at q_s/q_c = 0.25. Colorbar shows the thickness of the sediment cover, and white areas correspond to the exposed bedrock surface.

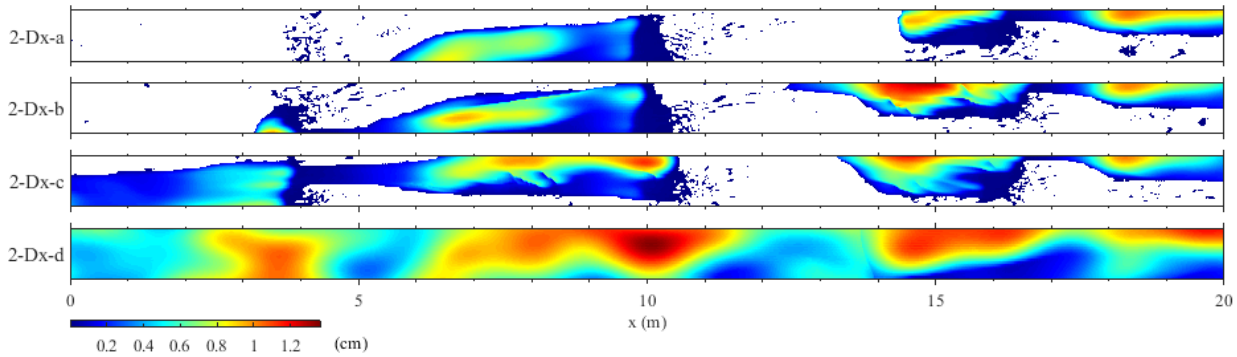

Figure 3.2. Plan view of Runs 2-Dx at equilibrium. The sediment is supplied at q_s/q_c = 0.25, 0.5, 0.75, and 1.0, from top to bottom. Colorbar shows the thickness of the sediment cover, and white areas correspond to the exposed bedrock surface.

end at the constant flux of 350 g/s, equating to the channel sediment transport capacity. The sediment tends to deposit on the stoss side of the bedrock mounds where low flow velocity results in low Froude number, shear stress, and sediment transport capacity. The gravels deposited on the bed form small patches which grow in size as they move downstream. The migrating alluvial patches bypass the high bedrock peaks by moving through the topographic lows. The upstream perturbation of sediment distribution triggers the formation of a sediment strip shifting from one

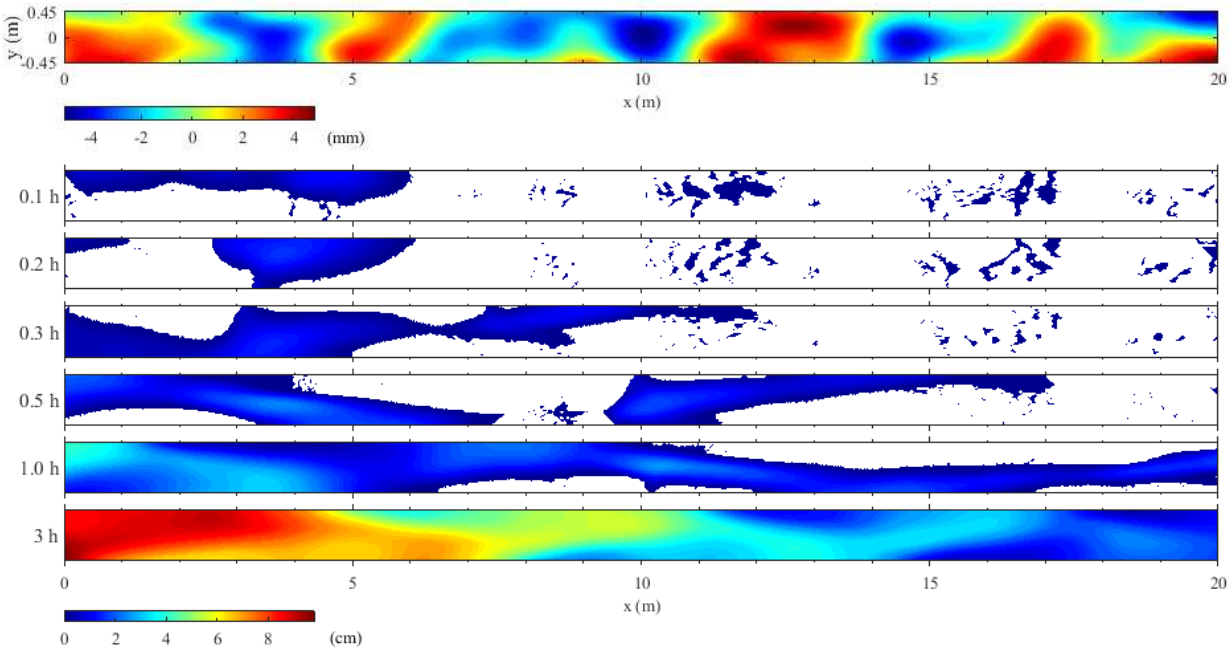

Figure 3.3. Plan view of bedrock topography (top). Colorbar scale indicates the detrended bed elevation. Simulated bed evolution of Run 2-Bx with $q_s/q_c = 1$ (bottom). Colorbar shows the thickness of the sediment cover, and white areas correspond to the exposed bedrock surface.

side to the other side of the channel, and the entire channel bed is covered with sediment eventually. Complete alluviation of the bedrock bed begins from the upstream end of the channel, and alternate bar patterns form as sediment moves across the channel.

Unlike the lower-slope runs of 2-Dx, simulations for 2-Ax ($S = 0.0115$) and 2-Bx ($S = 0.02$) were not able to achieve persistent alluvial cover for sediment supplies less than the transport capacity. Figure 3.4a demonstrates that the fraction of exposed bedrock surface varies with the sediment supply to transport capacity ratio in the initially bare bedrock channel. In steep-slope channels ($S \geq 0.0115$) without preexisting sediment, the bedrock bed remains fully exposed until the sediment supply rate is less than the channel sediment transport capacity. When the sediment supply momentarily exceeds the threshold value, the entire bedrock bed is completely covered by sediment, so-called runaway alluviation. In contrast, in the lower slope channel ($S = 0.003$, Run 2-

Dx), an increase in the sediment supply results in the expansion of the alluvial area, thus the gradual decrease in the fraction of bedrock exposure. These results are qualitatively and quantitatively similar to the observations of Chatanantavet and Parker [2008], whose experimental results are plotted alongside ours on the same figure (Figure 3.4).

3.3.2. Simulations with initial alluvial cover and varying slope

Figure 3.4b presents the agreement between the model-predicted and experimentally observed relationships between bedrock exposure fraction and sediment supply in channels with initial sediment cover. In a steeper slope channel (S = 0.02, Run 2-B), the bedrock is completely exposed when the sediment supply to transport capacity rate is less than 0.4. However, a linear relationship between the extent of sediment cover and sediment supply is exhibited when the sediment supply exceeds the threshold value (q_s/q_c > 0.6). As the channel slope decreases (Run 2-A), the threshold sediment capacity that triggers the linear relationship between sediment cover fraction and sediment supply ratio decreases. In a channel slope of 0.0115, the linear relationship is observed throughout the entire range of q_s/q_c that the fraction of bedrock exposure increases gradually as the sediment supply to capacity ratio decreases.

3.3.3. Simulations with various initial sediment layer thickness

The simulations of Runs 2-B2 and 2-B2-a to 2-B2-c are conducted to explore the effect of antecedent sediment layer thickness on alluvial patterns. Figure 3.5 shows the time evolution of (a) bedrock exposure and (b) averaged alluvial thickness in the 2 % slope channel. The initial sediment cover thickness varies between 1 to 6 cm while the sediment flux of 66 g/s is constantly supplied. In the simulation starting with 1 cm sediment cover thickness, the sediment quickly

erodes and washes out from the channel. The simulations with 2 cm or higher initial alluvial thickness present that the fraction of bedrock exposure increases gradually and converges approximately at 0.4. The mean alluvial layer thickness calculated from the area covered with sediment only tends to move toward 2 cm when the initial cover thickness equals or exceeds 2 cm.

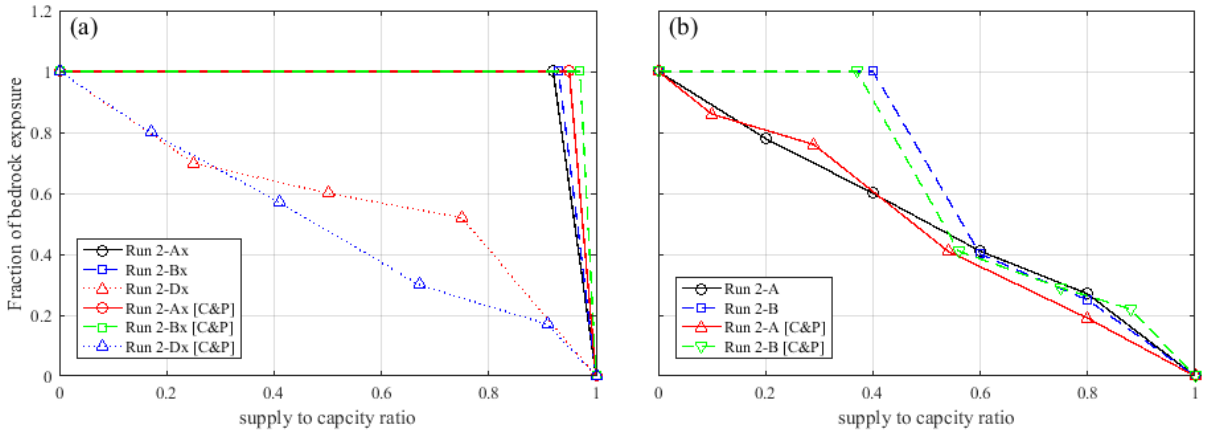

Figure 3.4. Results from the numerical simulations and flume experiments [Chatanantavet and Parker, 2008] of the fraction of bedrock exposure with varying sediment supply to transport capacity ratio for the simulations commenced from (a) bare bedrock channel and (b) alluvial channel.

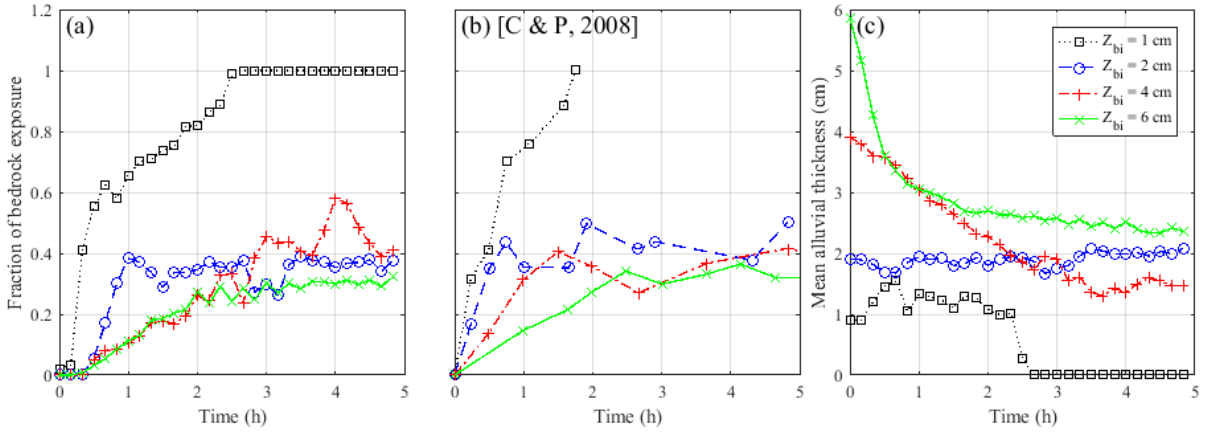

Figure 3.5. The time evolution of the (a) fraction of bedrock exposure from numerical simulations, (b) flume experiments [Chatanantavet and Parker, 2008], and (c) alluvial cover thickness averaged over the covered area only. The Runs of 2-B2-a, 2-B2, 2-B2-b, and 2-B2-c correspond to the initial cover thickness of 1, 2, 4, and 6 cm, respectively.

3.4. Discussion

Our results replicated several phenomena observed in the Chatanantavet and Parker [2008] experiments: 1) runaway alluviation for high-slope channels with no initial sediment cover, and gradual alluviation for low-slope channels with no initial sediment cover (Figure 3.4a), 2) a threshold sediment supply for higher-slope channels with the initial cover below which sediment washes out, but above which a linear relationship between sediment supply and fraction exposure develops (Figure 3.4b), and 3) a threshold initial sediment cover thickness above which quasi-steady sediment cover develops, but below which full bedrock exposure and sediment washout occurs. Here, we would like to use the model's complete description of the hydrodynamic and sediment transport conditions throughout the experiments to explain why these phenomena occurred.

Previous studies on sediment transport in the mixed bedrock-alluvial channel have focused on the fraction of bedrock exposure as an indicator of alluvial patterns [Chatanantavet and Parker, 2008; Hodge and Hoey, 2012; Johnson, 2014; Mishra and Inoue, 2020]. Research has shown that the channel slope, bedrock configuration and roughness, and antecedent channel alluviation condition affect the fraction of bedrock exposure. In our simulations, we explore the known drivers to investigate the root cause and detailed mechanisms of bedrock alluviation patterns using the flow field and sediment transport variables.

3.4.1. Runaway alluviation vs. gradual alluviation

The gradual decrease in the fraction of bedrock exposed with increasing sediment supply at the low-slope (2-Dx) condition, and the runaway alluviation at higher slopes where persistent (total) sediment cover occurred only at sediment supply greater than the transport capacity, with complete bedrock exposure at sediment supplies below that value, was observed in both our

numerical simulations and in the experiments of Chatanantavet and Parker [2008]. Chatanantavet and Parker [2008] suggested that this phenomenon may be in part due to sediment grain interactions, such that at low slopes, frequent grain collisions lead to the development of alluvial patches, which then increase local roughness and grow in size, whereas at higher slopes those collisions may be less frequent and less likely to develop incipient patches. A series of CA model runs with varying grain entrainment probability on bedrock and alluvial surfaces suggest that the much higher grain entrainment probability on the bedrock surface than the alluvial surface is a key factor of runaway alluviation [Hodge and Hoey, 2012].

Our model treats sediment transport as a continuum and is therefore not able to model grain interactions directly, but it still exhibited the same sort of slope-dependent relationship between gradual vs. runaway alluviation. Here, we suggest this is a result of the development of transcritical flows over bare low-slope beds, but not in higher-slope channels.

Figure 3.6 shows the Froude numbers calculated in the bare bedrock channel before feeding sediment at the inlet for the Runs 2-Ax, 2-Bx, and 2-Dx. The flow is supercritical in steep slope channels (2-Ax and 2-Bx), while locally subcritical flow is observed in lower slope channels (2-Dx). The flow field variables and shear stress result in a low sediment transport capacity where the flow is subcritical in the low-slope channel (Figure 3.7). These subcritical zones become areas of deposition, inducing a cascade of local changes in roughness, velocity, shear stress, and critical dimensionless shear stress which permit the growth of alluvial patches. However, in the steep slope channels, the large sediment transport capacity produced by high flow velocity and shear stress results in the particles passing through the channel reach without ever residing on the bed when the sediment supply is less than the transport capacity (Figure 3.4a).

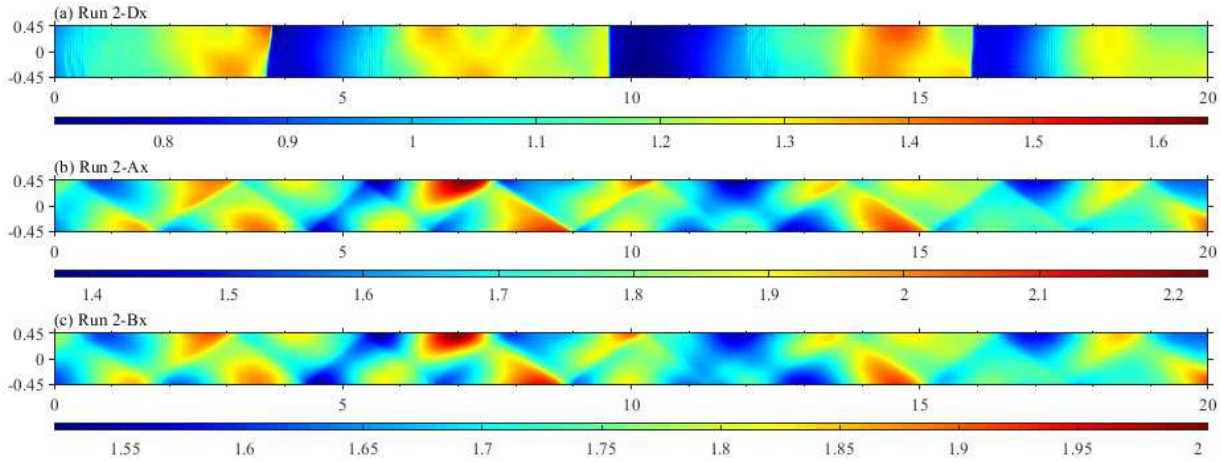

Figure 3.6. Initially calculated Froude number for Runs (a) 2-Dx, (b) 2-Ax, and (c) 2-Bx in bare bedrock channel. Colorbars indicate the scale of computed values, respectively.

Thus, while grain interactions and roughness feedbacks may play a role in developing persistent alluvial sediment cover at below-capacity sediment supply in low-slope channels, the specific flow field – especially the presence of regions of transcritical flow – can be an important control on this behavior.

3.4.2. Sediment supply threshold for persistent alluvial patches

The 2 % slope channel simulations with 2 cm initial cover thickness (Runs 2-B1, 2-B2, 2-B3, and 2-B4) show sediment washing out when the sediment supply rate is less than the threshold capacity of about $q_s/q_c = 0.4$. The sediment forms alternate bars that produce additional resistance to the flow. The increased form drag roughness competes with decreased bed surface roughness due to exposed bedrock beds. The channel experiences complete bedrock exposure when the sediment supply does not meet the required amount to maintain the bedform. In other words, the sediment supplied to the system is redistributed to create bedforms which increase overall

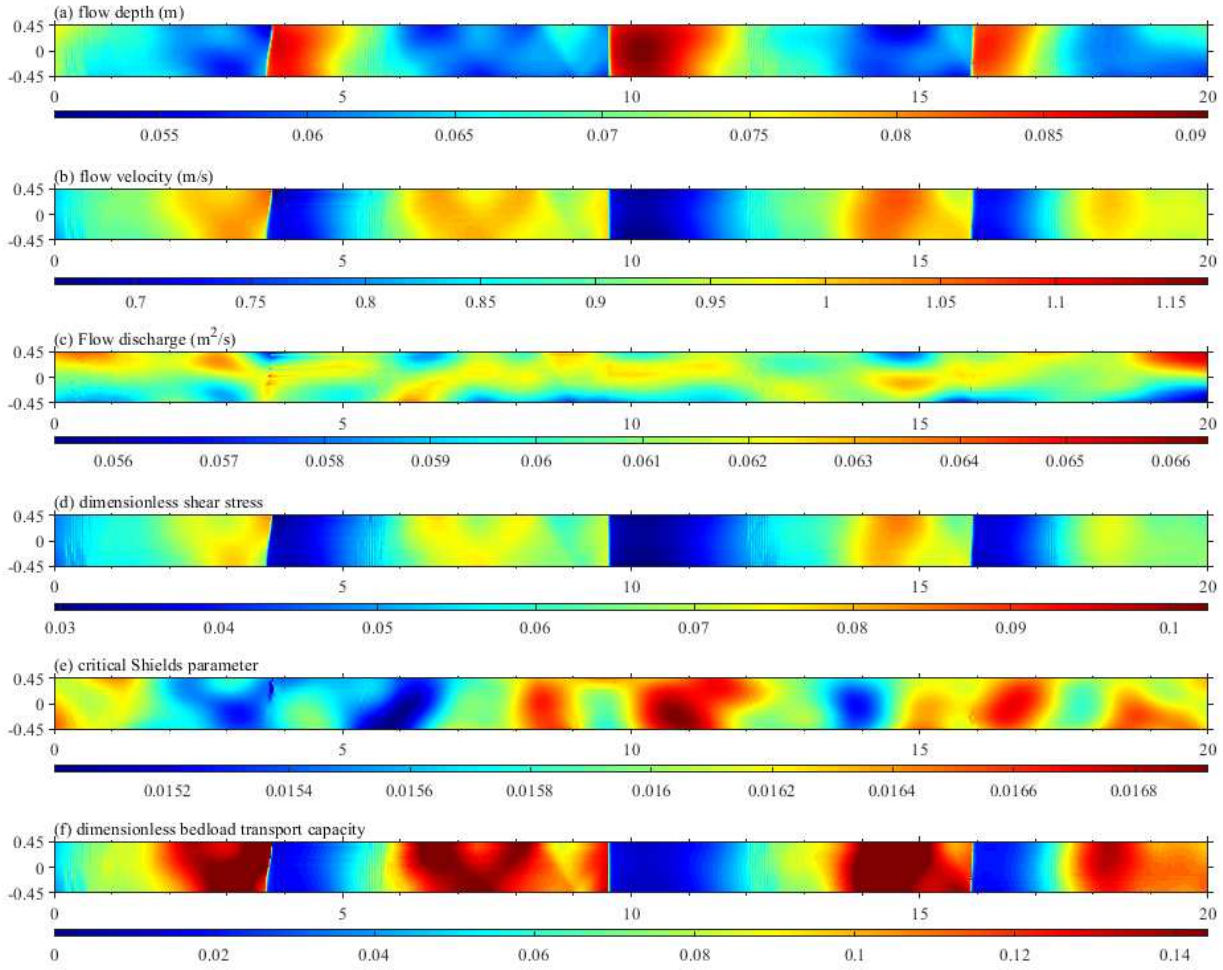

Figure 3.7. Initially calculated variables in bare bedrock channel for the Run 2-Dx: (a) flow depth, (b) flow velocity, (c) flow discharge, (d) dimensionless shear stress, (e) critical Shields parameter, and (f) dimensionless bed load transport capacity. Colorbars indicate the scale of computed values, respectively.

roughness and encourage sediment deposition and persistence of the alluvial cover; if the supply is insufficient to build the bedforms, the overall roughness decreases as bedrock becomes exposed and all of the sediment washes out (Figure 3.8).

Similar mechanisms explain the relationship between the initial thickness of sediment cover and the development of persistent alluvial cover as opposed to sediment washout at below-threshold initial thicknesses (Figure 3.5). The 1.15 % slope channel simulations with 1.5 cm initial

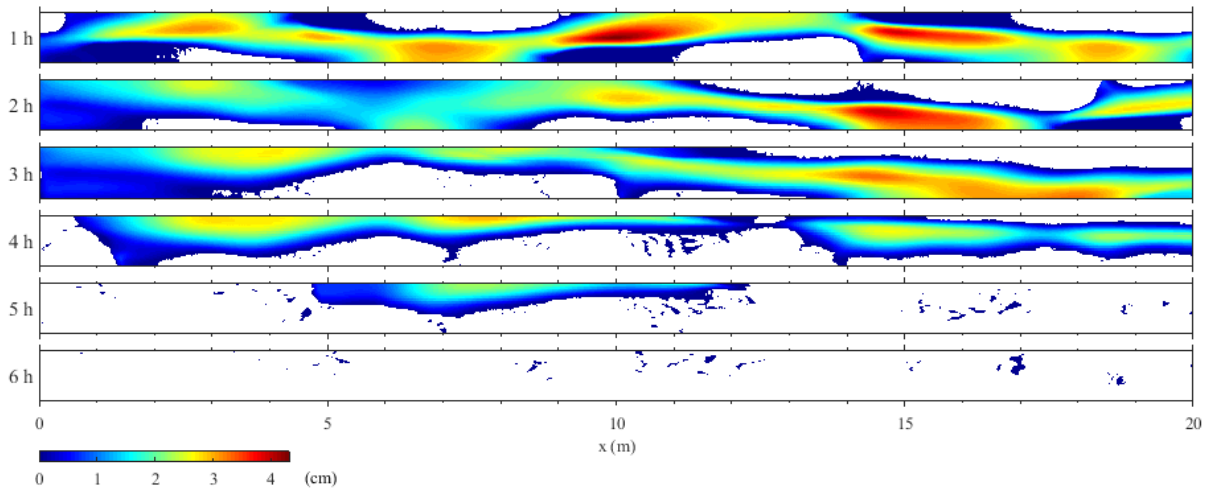

Figure 3.8. Simulated bed evolution of Run 2-B1 with q_s/q_c = 0.4. Colorbar shows the thickness of the sediment cover, and white areas correspond to the exposed bedrock surface.

cover thickness (Runs 2-A1 through 2-A5) show the linear relationship between the fraction cover and sediment supply to transport capacity. Transcritical flow is observed in this simulation (Figure 3.9). The flow is subcritical in the alluvial area and supercritical over the bedrock surface. The sediment forms a series of discrete sediment patches with a thin layer rather than a continuous strip of sediment. The subcritical flow promotes the thin layer of alluvial patches to form even in low sediment supply channels.

Figure 3.10 shows how roughness changes from the initial value of grain and sediment transport roughness, form drag, and total hydraulic roughness through time. The non-bedform roughness gradually decreases as bedrock exposure increases for all Runs of 2-B2. However, the bedform roughness of Runs 2-B2, 2-B2-b, and 2-B2-c increases to 5 mm at the equilibrium state, whereas the bedform roughness of Run 2-B2-a increases at the early stage and decreases back to 0. The changes in total roughness height indicate that the channel initially requires a thicker sediment cover layer than the minimum value to develop bars and maintain alluvial strips, or sediment washing out occurs.

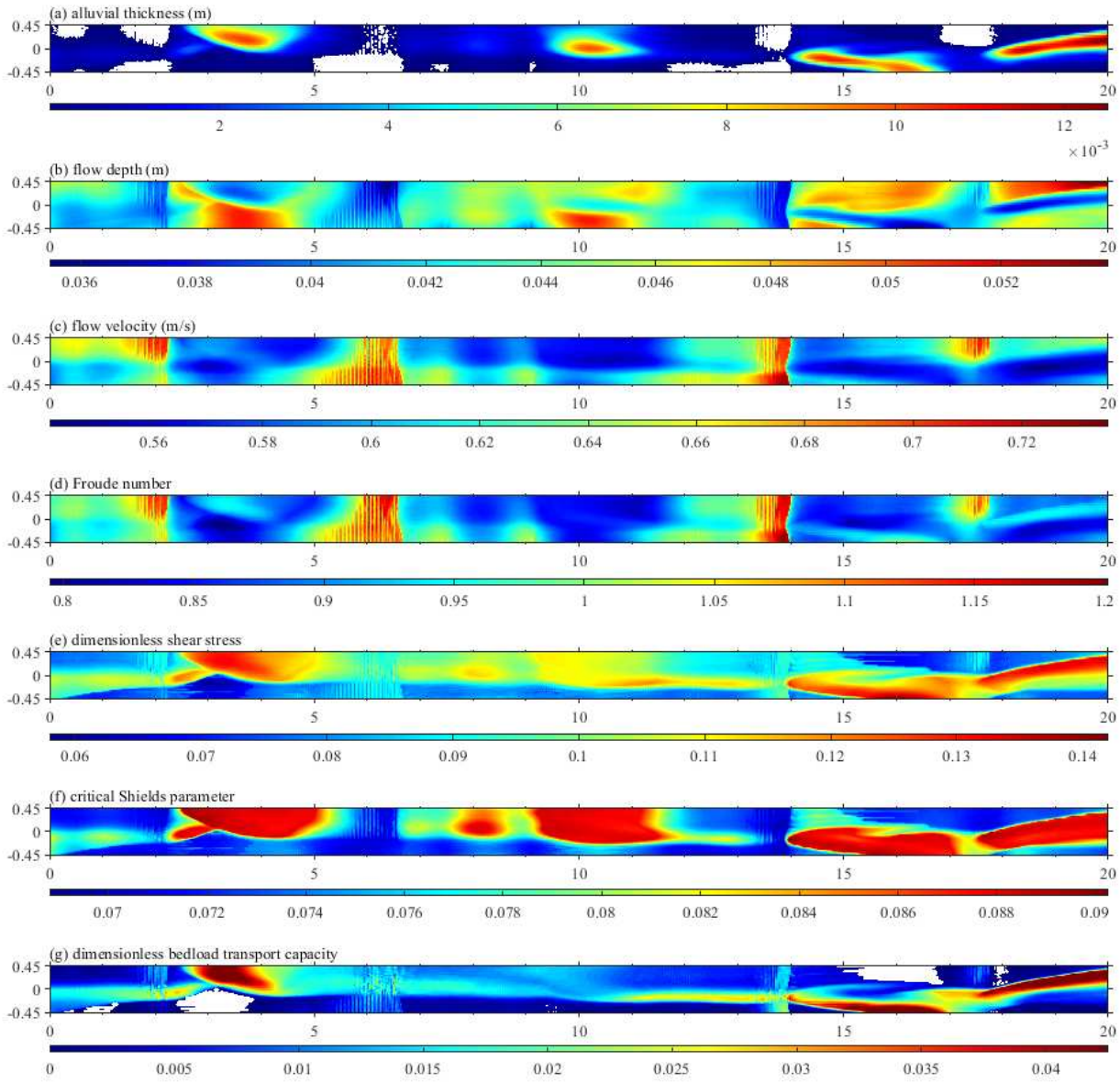

Figure 3.9. Simulation results commenced from alluvial channel for the Run 2-A2 at t = 5 h: (a) alluvial thickness, (b) flow depth, (c) flow velocity, (d) Froude number, (e) dimensionless shear stress, (f) critical Shields parameter, and (g) dimensionless bed load transport capacity. Colorbars indicate the scale of computed values, respectively. White areas correspond to (a) the exposed bedrock surface and (g) no bed load transport.

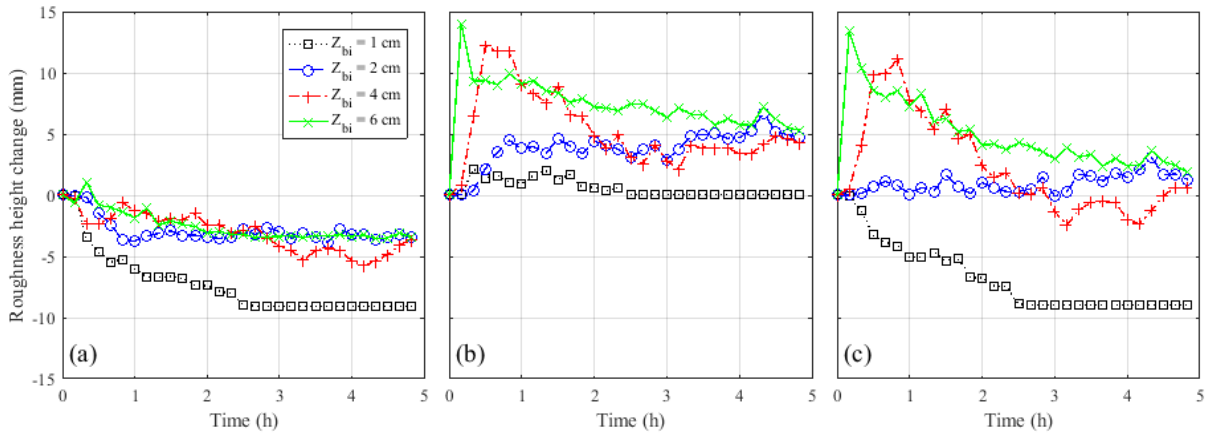

Figure 3.10. The time evolution of roughness difference from the initial roughness value: (a) bed surface roughness, (b) bedform roughness, and (c) total hydraulic roughness. The Runs of 2-B2-a, 2-B2, 2-B2-b, and 2-B2-c correspond to the initial cover thickness of 1, 2, 4, and 6 cm, respectively.

3.5. Conclusions

We used a two-dimensional morphodynamic model to conduct a series of numerical experiments in the mixed bedrock-alluvial channel. This study explores the interaction between bedrock alluviation and morphological evolution. Simulations with varying sediment supply are conducted in different slope and antecedent channel conditions. The model replicated observations from a mixed bedrock-alluvial experiment [Chatanantavet and Parker, 2008], including a) the relationship between channel slope and gradual vs. runaway alluviation, b) the slope-dependent sediment supply threshold for development of persistent alluvial cover, c) the relationship between decreasing bedrock exposure and increasing sediment supply, and d) the development of constant alluvial cover thickness regardless of initial sediment thickness, provided the initial thickness exceeds a minimum value necessary to maintain bedform dimensions.

The model results provide physical insight on the mechanisms responsible for these phenomena. Transcritical flow plays an important role in initiating sediment deposition over initially bare bedrock, and the development of transcritical zones in low-slope simulations but not high-

slope simulations may explain the apparent slope dependence of runaway alluviation. Persistent sediment cover in high-slope channels is possible when rough alluvial surfaces balance the extent of lower-roughness bedrock surfaces, and steeper channels require higher sediment supply to exceed an apparent threshold where that balance can occur.

CHAPTER 4

CONCLUSIONS

In this study, a morphodynamic model is developed to explore the dynamics and mechanisms of sediment transport and alluvial cover in mixed bedrock-alluvial channels. The new 2D morphodynamic model overcomes limitations present in existing models and employs composite roughness, partitioned into surface roughness, form drag, near-bed sediment transport roughness, and ripple factor. Our model tested its capability to predict the flow field, sediment transport, and bed evolution in alluvial and bedrock channels. The computed results of alternate bar characteristics and alluvial patterns are compared to the observed laboratory data. The model performs well for bedform development and migration in the alluvial channel and alluvial patch formation and evolution in mixed-bedrock alluvial channels. Additional simulations showed that fully accounting for form drag, sediment transport roughness, grain roughness, and correcting stress with a ripple factor are critical when modeling conditions in mixed bedrock-alluvial rivers.

Beyond reproducing flume experiments, the present work provides important insight on morphodynamic processes in mixed bedrock-alluvial channels. Simulations conducted in bare bedrock steep slope channels (S = 0.0115 and 0.02) show runaway alluviation as sediment supply momentarily exceeds transport capacity. In contrast, a gradual alluviation pattern is observed as the ratio of sediment supply to sediment transport increases in the low slope channel (S = 0.003). However, the simulations commenced from the alluvial channel display a linear relationship between the amount of bedrock exposed and sediment supply to transport capacity ratio in the low slope channel (S = 0.0115). The sediment is stripped in the steep slope channel (S = 0.02), and the bedrock becomes completely exposed where the sediment supply is less than the threshold

sediment transport. The linear relationship holds where the sediment supply exceeds the threshold transport capacity. The simulations performed in a steep slope channel (S = 0.02) with a thicker than threshold initial sediment cover layer exhibits the convergence of fraction bedrock covered (P_c = 0.6) approximately the sediment supply to transport capacity ratio (q_s/q_c = 0.6). The mean sediment cover thickness becomes 2 cm when the initial cover layer is thicker than the threshold thickness.

These phenomena, which have been observed in flume experiments and have now been numerically simulated, result from the combined effects of the flow pattern, the roughness difference between the bedrock and alluvial surfaces, roughness patterns produced by the channel, bedforms, and bed load transport, and the preexisting channel alluviation condition. Numerical simulations with the direct linkage between the flow fields, sediment transport, and bed evolution provide advanced explanations of where and how much sediment is deposited on the bedrock bed. In addition, the characterization of 3D bedforms and their effects on flow resistance, roughness induced by the grain movements, and correction to the shear stress to account for reduced form drag effects on near-bed sediment transport promote the model predictability in a wide range of slope, sediment supply, and antecedent channel alluviation condition.

In low slope channels, near-critical and transcritical flows are generated and form local low-stress regions that enable deposition and growth of alluvial patches, where the downstream flow velocity is low and bed elevation is low. These patches expand with increasing sediment supply, producing a linear relationship between the fraction of bedrock exposure and the ratio of sediment supply to transport capacity.

In the threshold slope channel (S = 0.0115), the roughness difference between the bedrock and alluvial surface exhibits a distinctive alluviation pattern depending on the antecedent channel

condition. The higher grain roughness generates subcritical flows in the initial alluvial channel. Transcritical flow develops as bedrock is exposed at low sediment supply, and a linear relationship between the fraction of bedrock exposure and sediment supply to transport capacity ratio is presented. However, the initial bedrock channel maintains supercritical flow until the bed is completely alluviated due to the high bed load transport rate in the bedrock surface.

The roughness between the bedrock and the alluvial surface is a primary driver of the alluvial pattern in steeper slope channels. When starting with an initially bare bed, the shear stress and sediment transport capacity over the bedrock produce throughput bed load, such that sediment particles saltate without ever residing on the bed until the sediment supply exceeds the transport capacity, when runaway alluviation occurs. In order to attain a persistent strip of alluvial cover in the steep slope channel, a sufficient amount of preexisting alluvium and sediment supply is necessary to develop incipient bedforms. These then generate increasing bedform roughness, which counteracts the reduced surface roughness due to the exposed bedrock surface and creates a delicate balance where sediment cover can persist.

In the numerical simulations bed roughness and critical shear stress are adjusted depending on the flow discharge and sediment transport capacity measured from the flume experiments. Further studies to explore the dynamics and mechanisms of sediment transport and alluviation pattern in field sites can be conducted with field measurements of flow discharge and sediment transport capacity.

The model has provided mechanistic insight on the development of alluvial patterns in mixed bedrock-alluvial channels. It therefore provides a foundation for future research, which may include incorporation of 3D nature of flow fields, suspended sediment transport, models for bedrock erosion by bed load and suspended load, and/or transport of sediment mixtures.

REFERENCES

Ashida, K., & Michiue, M. (1972). Hydraulic Resistance of Flow in an Alluvia Bed and Bed Load Transport Rate. *Proceedings of Japan Society of Civil Engineers*, 59–69. https://scirp.org/reference/referencespapers.aspx?referenceid=1312271

Bernini, a., Caleffi, V., & Valiani, A. (2006). Numerical Modelling of Alternate Bars in Shallow Channels. *Braided Rivers*, 153–175. https://doi.org/10.1002/9781444304374.ch7

Booth, D. B., & Bledsoe, B. P. (2009). Streams and Urbanization. In *The Water Environment of Cities* (pp. 93–123). https://doi.org/10.1007/978-0-387-84891-4_6

Buffington, J. M., Montgomery, D. R., & Greenberg, H. M. (2004). Basin-scale availability of salmonid spawning gravel as influenced by channel type and hydraulic roughness in mountain catchments. *Canadian Journal of Fisheries and Aquatic Sciences*, *61*(11), 2085–2096. https://doi.org/10.1139/f04-141

Calantoni, J. (2002). Discrete particle model for bedload sediment transport in the surf zone. North Carolina State University.

Chatanantavet, P., & Parker, G. (2008). Experimental study of bedrock channel alluviation under varied sediment supply and hydraulic conditions. *Water Resources Research*, *44*(12), 1–19. https://doi.org/10.1029/2007WR006581

Damgaard, J. S., Whitehouse, R. J. S., & Soulsby, R. L. (1997). Bed-Load Sediment Transport on Steep Longitudinal Slopes. *Journal of Hydraulic Engineering*, *123*(12), 1130–1138. https://doi.org/10.1061/(ASCE)0733-9429(1997)123:12(1130)

De Vries M. (1965). Considerations about non-steady bed-load transport in open channels. *Proc. 11th Int. Congr. IAHR, Delft, the Netherlands, 3-8*.

Defina, A. (2003). Numerical experiments on bar growth. *Water Resources Research*, *39*(4), 1–12. https://doi.org/10.1029/2002WR001455

Demeter, G. I., Sklar, L. S., & Davis, J. R. (2005). The influence of variable sediment supply and bed roughness on the spatial distribution of incision in a laboratory bedrock channel. *2005 Fall Meeting of the AGU*, 2004.

Detert, M., & Parker, G. (2010). Estimation of the Washout Depth of Fine Sediments from a Granular Bed. *Journal of Hydraulic Engineering*, *136*(10), 790–793. https://doi.org/10.1061/(ASCE)HY.1943-7900.0000263

Dietrich, W. E. (1982). Settling velocity of natural particles. *Water Resources Research*, *18*(6), 1615–1626. https://doi.org/10.1029/WR018i006p01615

Duan, J. G., & Julien, P. Y. (2005). Numerical simulation of the inception of channel meandering. *Earth Surface Processes and Landforms*, *30*(9), 1093–1110. https://doi.org/10.1002/esp.1264

Engelund, F. (1977). *Hydraulic resistance for flow over dunes.*

Finnegan, N. J., Sklar, L. S., & Fuller, T. K. (2007). Interplay of sediment supply, river incision, and channel morphology revealed by the transient evolution of an experimental bedrock channel. *Journal of Geophysical Research: Earth Surface*, *112*(3), 1–17. https://doi.org/10.1029/2006JF000569

Gasparini, N. M., Whipple, K. X., & Bras, R. L. (2007). Predictions of steady state and transient landscape morphology using sediment-flux-dependent river incision models. *Journal of Geophysical Research: Earth Surface*, *112*(3), 1–20. https://doi.org/10.1029/2006JF000567

Goode, J. R., & Wohl, E. (2010a). Coarse sediment transport in a bedrock channel with complex bed topography. *Water Resources Research*, *46*(11), 1–14. https://doi.org/10.1029/2010WR009078

Goode, J. R., & Wohl, E. (2010b). Substrate controls on the longitudinal profile of bedrock channels: Implications for reach-scale roughness. *Journal of Geophysical Research: Earth Surface*, *115*(3), 1–14. https://doi.org/10.1029/2008JF001188

Grant, W. D., & Madsen, O. S. (1982). Movable bed roughness in unsteady oscillatory flow. *Journal of Geophysical Research*, *87*(C1), 469–481. https://doi.org/10.1029/JC087iC01p00469

Hartshorn, K., Hovius, N., Dade, W. B., & Slingerland, R. L. (2002). Climate-driven bedrock incision in an active mountain belt. *Science*, *297*(5589), 2036–2038. https://doi.org/10.1126/science.1075078

Hodge, R. A., & Hoey, T. B. (2012). Upscaling from grain-scale processes to alluviation in bedrock channels using a cellular automaton model. *Journal of Geophysical Research: Earth Surface*, *117*(F1), n/a-n/a. https://doi.org/10.1029/2011JF002145

Hodge, R. A., & Hoey, T. B. (2016a). A Froude-scaled model of a bedrock-alluvial channel reach: 1. Hydraulics. *Journal of Geophysical Research: Earth Surface*, *121*(9), 1578–1596. https://doi.org/10.1002/2015JF003706

Hodge, R. A., & Hoey, T. B. (2016b). A Froude-scaled model of a bedrock-alluvial channel reach: 2. Sediment cover. *Journal of Geophysical Research: Earth Surface*, *121*(9), 1597–1618. https://doi.org/10.1002/2015JF003709

Howard, A. D. (1980). Thresholds in river regimes. In *Thresholds in Geomorphology* (pp. 227–258).

Howard, A. D. (1987). Modelling Fluvial Systems: Rock-, Gravel-, and Sand-bed Channels. In *River Channels: Environment and Process* (pp. 69–94).

Howard, A. D. (1998). Long profile development of bedrock channels: Interaction of weathering, mass wasting, bed erosion, and sediment transport. In K. J. Tinkler & E. E. Wohl (Eds.), *Rivers Over Rock: Fluvial Processes in Bedrock Channels* (Volume 107, pp. 297–319). https://doi.org/10.1029/GM107p0297

Howard, A. D., Dietrich, W. E., & Seidl, M. A. (1994). Modeling fluvial erosion on regional to continental scales. *Journal of Geophysical Research: Solid Earth*, *99*(B7), 13971–13986. https://doi.org/10.1029/94JB00744

Howard, A. D., & Kerby, G. (1983). Channel changes in badlands. *Geological Society of America Bulletin*, *94*(6), 739. https://doi.org/10.1130/0016-7606(1983)94<739:CCIB>2.0.CO;2

Huston, D., & Fox, J. F. (2016). Momentum-Impulse Model of Fine Sand Clogging Depth in Gravel Streambeds for Turbulent Open-Channel Flow. *Journal of Hydraulic Engineering*, *142*(2). https://doi.org/10.1061/(ASCE)HY.1943-7900.0001092

Ikeda, S. (1984). Prediction of Alternate Bar Wavelength and Height. *Journal of Hydraulic Engineering*, *110*(4), 371–386. https://doi.org/10.1061/(ASCE)0733-9429(1984)110:4(371)

Inoue, T, Iwasaki, T., Parker, G., Shimizu, Y., Izumi, N., Stark, C. P., & Funaki, J. (2016). Numerical Simulation of Effects of Sediment Supply on Bedrock Channel Morphology. *Journal of Hydraulic Engineering*, 04016014. https://doi.org/10.1061/(ASCE)HY.1943-7900.0001124

Inoue, Takuya, Izumi, N., Shimizu, Y., & Parker, G. (2014). Interaction among alluvial cover, bed roughness, and incision rate in purely bedrock and alluvial-bedrock channel. *Journal of Geophysical Research: Earth Surface*, *119*(10), 2123–2146. https://doi.org/10.1002/2014JF003133

Inoue, Takuya, & Nelson, J. M. (2020). An Experimental Study of Longitudinal Incisional Grooves in a Mixed Bedrock–Alluvial Channel. *Water Resources Research*, *56*(3). https://doi.org/10.1029/2019wr025410

Izumi, N., Yokokawa, M., & Parker, G. (2017). Incisional cyclic steps of permanent form in mixed bedrock-alluvial rivers. *Journal of Geophysical Research: Earth Surface*, *122*(1), 130–152. https://doi.org/10.1002/2016JF003847

Johnson, J. P. L. (2014). A surface roughness model for predicting alluvial cover and bed load transport rate in bedrock channels. *Journal of Geophysical Research: Earth Surface*, *119Johnson*(10), 2147–2173. https://doi.org/10.1002/2013JF003000

Johnson, J. P., & Whipple, K. X. (2007). Feedbacks between erosion and sediment transport in experimental bedrock channels. *Earth Surface Processes and Landforms*, *32*(7), 1048–1062. https://doi.org/10.1002/esp.1471

Knighton, D. (2014). *Fluvial Forms and Processes*. Routledge. https://doi.org/10.4324/9780203784662

Kostic, S., Sequeiros, O., Spinewine, B., & Parker, G. (2010). Cyclic steps: A phenomenon of supercritical shallow flow from the high mountains to the bottom of the ocean. Journal of Hydro-Environment Research, 3(4), 167–172. https://doi.org/10.1016/j.jher.2009.10.002

Kuhnle, R. A., Wren, D. G., Langendoen, E. J., & Rigby, J. R. (2013). Sand transport over an immobile gravel substrate. *Journal of Hydraulic Engineering*, *139*(2), 167–176. https://doi.org/10.1061/(ASCE)HY.1943-7900.0000615

Lamb, M. P., Dietrich, W. E., & Venditti, J. G. (2008). Is the critical shields stress for incipient sediment motion dependent on channel-bed slope? *Journal of Geophysical Research: Earth Surface*, *113*(2), 1–20. https://doi.org/10.1029/2007JF000831

Lamb, M. P., Finnegan, N. J., Scheingross, J. S., & Sklar, L. S. (2015). New insights into the mechanics of fluvial bedrock erosion through flume experiments and theory. *Geomorphology*, *244*, 33–55. https://doi.org/10.1016/j.geomorph.2015.03.003

Lanzoni, S. (2000a). Experiments on bar formation in a straight flume: 1. Uniform sediment. *Water Resources Research*, *36*(11), 3337–3349. https://doi.org/10.1029/2000WR900160

Lanzoni, S. (2000b). Experiments on bar formation in a straight flume: 2. Graded sediment. *Water Resources Research*, *36*(11), 3351–3363. https://doi.org/10.1029/2000WR900161

Lisle, T. E., & Hilton, S. (1992). The Volume Of Fine Sediment In Pools: An Index Of Sediment Supply In Gravel-Bed Streams. *Journal of the American Water Resources Association*, *28*(2), 371–383. https://doi.org/10.1111/j.1752-1688.1992.tb04003.x

Lisle, T. E., & Lewis, J. (1992). Effects of Sediment Transport on Survival of Salmonid Embryos in a Natural Stream: A Simulation Approach. *Canadian Journal of Fisheries and Aquatic Sciences*, *49*(11), 2337–2344. https://doi.org/10.1139/f92-257

Lisle, T. E., & Madej, M. a. (1992). Spatial Variation in Armouring in a Channel with High Sediment Supply. *Dynamics of Gravel-Bed Rivers*, 277–293. https://doi.org/10.1002/jhet.5570170102

Luu, L. X., Egashira, S., & Takebayashi, H. (2004). Investigation of Tan Chau Reach In Lower Mekong Using Field Data And Numerical Simulation. *PROCEEDINGS OF HYDRAULIC ENGINEERING*, *48*(5), 1057–1062. https://doi.org/10.2208/prohe.48.1057

Maddux, T. B., McLean, S. R., & Nelson, J. M. (2003). Turbulent flow over three-dimensional dunes: 2. Fluid and bed stresses. *Journal of Geophysical Research: Earth Surface*, *108*(F1), n/a-n/a. https://doi.org/10.1029/2003jf000018

Maddux, T. B., Nelson, J. M., & McLean, S. R. (2003). Turbulent flow over three-dimensional dunes: 1. Free surface and flow response. *Journal of Geophysical Research: Earth Surface*, *108*(F1), n/a-n/a. https://doi.org/10.1029/2003JF000017

Madej, M. A. (2001). Development of channel organization and roughness following sediment pulses in single-thread, gravel bed rivers. *Water Resources Research*, *37*(8), 2259–2272. https://doi.org/10.1029/2001WR000229

Massong, T. M., & Montgomery, D. R. (2000). Influence of sediment supply, lithology, and wood debris on the distribution of bedrock and alluvial channels. *Geological Society of America Bulletin*, *112*(4), 591–599. https://doi.org/10.1130/0016-7606(2000)112<591:IOSSLA>2.0.CO;2

McLean, S. R., Nelson, J. M., & Wolfe, S. R. (1994). Turbulence structure over two-dimensional bed forms: Implications for sediment transport. *Journal of Geophysical Research*, *99*(C6), 12729. https://doi.org/10.1029/94JC00571

Mendoza, A., Abad, J. D., Langendoen, E. J., Wang, D., Tassi, P., & Abderrezzak, K. E. K. (2017). Effect of Sediment Transport Boundary Conditions on the Numerical Modeling of Bed Morphodynamics. *Journal of Hydraulic Engineering*, *143*(4), 04016099. https://doi.org/10.1061/(ASCE)HY.1943-7900.0001208

Meyer-Peter, E., & Müller, R. (1948). Formulas for Bed-Load Transport. *Proceedings of the 2nd Meeting of the International Association of Hydraulic Research*, 39–64. https://doi.org/1948-06-07

Mishra, J., & Inoue, T. (2020). Alluvial cover on bedrock channels: applicability of existing models. *Earth Surface Dynamics*, *8*(3), 695–716. https://doi.org/10.5194/esurf-8-695-2020

Montgomery, D. R., Abbe, T. B., Buffington, J. M., Peterson, N. P., Schmidt, K. M., & Stock, J. D. (1996). Distribution of bedrock and alluvial channels in forested mountain drainage basins. In *Nature* (Vol. 381, Issue 6583, pp. 587–589). https://doi.org/10.1038/381587a0

Montgomery, D. R., & Buffington, J. M. (1997). Channel-reach morphology in mountain drainage basins. *Bulletin of the Geological Society of America*, *109*(5), 596–611. https://doi.org/10.1130/0016-7606(1997)109<0596:CRMIMD>2.3.CO

Murray, A. B., & Paola, C. (1997). Properties of a cellular braided-stream model. *Earth Surface Processes and Landforms*, *22*(11), 1001–1025. https://doi.org/10.1002/(SICI)1096-9837(199711)22:11<1001::AID-ESP798>3.0.CO;2-O

Nelson, J. M. (1990). The initial instability and finite-amplitude stability of alternate bars in straight channels. *Earth Science Reviews*, *29*(1–4), 97–115. https://doi.org/10.1016/0012-8252(0)90030-Y

Nelson, J. M., Bennett, J. P., & Wiele, S. M. (2003). Flow and sediment-transport modeling. *Tools in Fluvial Geomorphology*. https://doi.org/10.1002/0470868333.ch18

Nelson, J. M., & Smith, J. D. (1989). Mechanics of flow over ripples and dunes. *Journal of Geophysical Research*, *94*(C6), 8146. https://doi.org/10.1029/JC094iC06p08146

Nelson, P. A., Bolla Pittaluga, M., & Seminara, G. (2014). Finite amplitude bars in mixed bedrock-alluvial channels. *Journal of Geophysical Research: Earth Surface*, *119*(3), 566–587. https://doi.org/10.1002/2013JF002957

Nelson, P. A., McDonald, R. R., Nelson, J. M., & Dietrich, W. E. (2015a). Coevolution of bed surface patchiness and channel morphology: 1. Mechanisms of forced patch formation. *Journal of Geophysical Research F: Earth Surface*, *120*(9), 1687–1707. https://doi.org/10.1002/2014JF003428

Nelson, P. A., McDonald, R. R., Nelson, J. M., & Dietrich, W. E. (2015b). Coevolution of bed surface patchiness and channel morphology: 2. Numerical experiments. *Journal of Geophysical Research F: Earth Surface*, *120*(9), 1708–1723. https://doi.org/10.1002/2014JF003429

Nelson, P. A., & Seminara, G. (2011). Modeling the evolution of bedrock channel shape with erosion from saltating bed load. *Geophysical Research Letters*, *38*(17), 1–5. https://doi.org/10.1029/2011GL048628

Nelson, P. A., & Seminara, G. (2012). A theoretical framework for the morphodynamics of bedrock channels. *Geophysical Research Letters*, *39*(6), 1–7. https://doi.org/10.1029/2011GL050806

Nittrouer, J. A., Mohrig, D., Allison, M. A., & Peyret, A. P. B. (2011). The lowermost Mississippi River: A mixed bedrock-alluvial channel. *Sedimentology*, *58*(7), 1914–1934. https://doi.org/10.1111/j.1365-3091.2011.01245.x

Parker, G., & Klingeman, P. C. (1982). On why gravel bed streams are paved. *Water Resources Research*, *18*(5), 1409–1423. https://doi.org/10.1029/WR018i005p01409

Parker, G., & Toro-Escobar, C. M. (2002). Equal mobility of gravel in streams: The remains of the day. *Water Resources Research*, *38*(11), 46-1-46–48. https://doi.org/10.1029/2001wr000669

Qian, H., Cao, Z., Liu, H., & Pender, G. (2017). Numerical modelling of alternate bar formation, development and sediment sorting in straight channels. *Earth Surface Processes and Landforms*, *42*(4), 555–574. https://doi.org/10.1002/esp.3988

Raudkivi, A. J. (1997). Ripples on Stream Bed. *Journal of Hydraulic Engineering*, *123*(1), 58–64. https://doi.org/10.1061/(ASCE)0733-9429(1997)123:1(58)

Ribberink, J. S. (1987). Mathematical modelling of one-dimensional morphological changes in rivers with non-uniform sediment. *Communications on Hydraulic & Geotechnical Engineering - Delft University of Technology*, *87–2*.

Schuurman, F., Marra, W. A., & Kleinhans, M. G. (2013). Physics-based modeling of large braided sand-bed rivers: Bar pattern formation, dynamics, and sensitivity. *Journal of Geophysical Research: Earth Surface*, *118*(4), 2509–2527. https://doi.org/10.1002/2013JF002896

Seidl, M., & Dietrich, W. (1992). The problem of channel erosion into bedrock. *Catena*, *23*(Supplement), 101–104.

Sklar, L., & Dietrich, W. E. (1998). River longitudinal profiles and bedrock incision models: Stream power and the influence of sediment supply. In K. J. Tinkler & E. E. Wohl (Eds.), *Rivers Over Rock: Fluvial Processes in Bedrock Channels* (Volume 107, pp. 237–260). https://doi.org/10.1029/GM107p0237

Sklar, L. S., & Dietrich, W. E. (2001). Sediment and rock strength controls on river incision into bedrock. *Geology*, *29*(12), 1087. https://doi.org/10.1130/0091-7613(2001)029<1087:SARSCO>2.0.CO;2

Sklar, L. S., & Dietrich, W. E. (2004). A mechanistic model for river incision into bedrock by saltating bed load. *Water Resources Research*, *40*(6), 1–21. https://doi.org/10.1029/2003WR002496

Smith, J. D., & Mclean, S. R. (1984). A Model for Flow in Meandering Streams. *Water Resources Research*, *20*(9), 1301–1315. https://doi.org/10.1029/WR020i009p01301

Smith, J. D., & McLean, S. R. (1977). Spatially averaged flow over a wavy surface. *Journal of Geophysical Research*, *82*(12), 1735. https://doi.org/10.1029/JC082i012p01735

Stansby, P. (2003). A mixing-length model for shallow turbulent wakes. *Journal of Fluid Mechanics*, *495*, 369–384. https://doi.org/10.1017/S0022112003006384

Struiksma, N. (1985). Prediction of 2-D bed topography in rivers. *Journal of Hydraulic Engineering*, *111*(8), 1169–1182. https://doi.org/10.1061/(ASCE)0733-9429(1985)111:8(1169)

Talmon, A. M., Struiksma, N., & Van Mierlo, M. C. L. M. (1995). Laboratory measurements of the direction of sediment transport on transverse alluvial-bed slopes. *Journal of Hydraulic Research*, *33*(4), 495–517. https://doi.org/10.1080/00221689509498657

Tinkler, K., & Wohl, E. (1998). *A primer on bedrock channels* (pp. 1–18). https://doi.org/10.1029/GM107p0001

Toro, E. F. (1992a). The weighted average flux method applied to the Euler equations. *Philosophical Transactions of the Royal Society of London. Series A: Physical and Engineering Sciences*, *341*(1662), 499–530. https://doi.org/10.1098/rsta.1992.0113

Toro, E. F. (1992b). Riemann Problems and the WAF Method for Solving the Two-Dimensional Shallow Water Equations. *Philosophical Transactions of the Royal Society A: Mathematical, Physical and Engineering Sciences*, *338*(1649), 43–68. https://doi.org/10.1098/rsta.1992.0002

Toro, E. F., Spruce, M., & Speares, W. (1994). Restoration of the contact surface in the HLL-Riemann solver. *Shock Waves*, *4*(1), 25–34. https://doi.org/10.1007/BF01414629

Toro, Eleuterio F. (2009). The HLL and HLLC Riemann Solvers. In *Riemann Solvers and Numerical Methods for Fluid Dynamics* (pp. 315–344). Springer Berlin Heidelberg. https://doi.org/10.1007/b79761_10

Tubino, M., Repetto, R., & Zolezzi, G. (1999). Free bars in rivers. *Journal of Hydraulic Research*, *37*(6), 759–775. https://doi.org/10.1080/00221689909498510

Turowski, J. M., Hovius, N., Meng-Long, H., Lague, D., & Men-Chiang, C. (2008). Distribution of erosion across bedrock channels. *Earth Surface Processes and Landforms*, *33*(3), 353–363. https://doi.org/10.1002/esp.1559

Turowski, J. M., Hovius, N., Wilson, A., & Horng, M. J. (2008). Hydraulic geometry, river sediment and the definition of bedrock channels. *Geomorphology*, *99*(1–4), 26–38. https://doi.org/10.1016/j.geomorph.2007.10.001

Turowski, J. M., Lague, D., & Hovius, N. (2007). Cover effect in bedrock abrasion: A new derivation and its implications for the modeling of bedrock channel morphology. *Journal of Geophysical Research: Earth Surface*, *112*(4), 1–16. https://doi.org/10.1029/2006JF000697

Turowski, J. M., & Rickenmann, D. (2009). Tools and cover effects in bedload transport observations in the Pitzbach, Austria. *Earth Surface Processes and Landforms*, *34*(1), 26–37. https://doi.org/10.1002/esp.1686

Van der Meer, C., Mosselman, E., Sloff, K., Jager, B., Zolezzi, G., & Tubino, M. (2011). Numerical simulations of upstream and downstream overdeepening. *River, Coastal and Estuarine Morphodynamics*, *1967*, 1721–1729.

van Rijn, L. C. (1982). Equivalent Roughness of Alluvial Bed. *Journal of the Hydraulics Division*, *108*(10), 1215–1218. https://doi.org/10.1061/JYCEAJ.0005917

van Rijn, L. C. (1984). Sediment Transport, Part III: Bed forms and Alluvial Roughness. *Journal of Hydraulic Engineering*, *110*(12), 1733–1754. https://doi.org/10.1061/(ASCE)0733-9429(1984)110:12(1733)

Vanoui, V. A., & Hwang, L.-S. (1967). Relation Between Bed Forms and Friction in Streams. *Journal of the Hydraulics Division*, *93*(3), 121–144. https://doi.org/10.1061/jyceaj.0001607

Vermeer, K. (1986). The ripple factor in sediment transport equations. *Rep. R657/M1314-V*.

Whipple, K. X. (2001). Fluvial Landscape Response Time: How Plausible Is Steady-State Denudation? *American Journal of Science*, *301*(4–5), 313–325. https://doi.org/10.2475/ajs.301.4-5.313

Whipple, K. X. (2004). Bedrock rivers and the geomorphology of active orogens. In *Annual Review of Earth and Planetary Sciences* (Vol. 32, Issue 1, pp. 151–185). https://doi.org/10.1146/annurev.earth.32.101802.120356

Whipple, K. X., & Tucker, G. E. (1999). Dynamics of the stream-power river incision model: Implications for height limits of mountain ranges, landscape response timescales, and research needs. *Journal of Geophysical Research: Solid Earth*, *104*(B8), 17661–17674. https://doi.org/10.1029/1999JB900120

Whipple, K. X., & Tucker, G. E. (2002). Implications of sediment-flux-dependent river incision models for landscape evolution. *Journal of Geophysical Research*, *107*(B2), 2039. https://doi.org/10.1029/2000JB000044

Wiberg, P. L., & Nelson, J. M. (1992). Unidirectional flow over asymmetric and symmetric ripples. *Journal of Geophysical Research*, *97*(C8), 12745. https://doi.org/10.1029/92JC01228

Wiberg, P. L., & Rubin, D. M. (1989). Bed roughness produced by saltating sediment. *Journal of Geophysical Research*, *94*(C4), 5011. https://doi.org/10.1029/JC094iC04p05011

Wiberg, P. L., & Smith, J. D. (1987). Calculations of the critical shear stress for motion of uniform and heterogeneous sediments. *Water Resources Research*, *23*(8), 1471–1480. https://doi.org/10.1029/WR023i008p01471

Wohl, E. E. (1993). Bedrock Channel Incision along Piccaninny Creek, Australia. *The Journal of Geology*, *101*(6), 749–761. https://doi.org/10.1086/648272

Wong, M., Parker, G., DeVries, P., Brown, T. M., & Burges, S. J. (2007). Experiments on dispersion of tracer stones under lower-regime plane-bed equilibrium bed load transport. *Water Resources Research*, *43*(3), n/a-n/a. https://doi.org/10.1029/2006WR005172

Wu, F. C., Shao, Y. C., & Chen, Y. C. (2011). Quantifying the forcing effect of channel width variations on free bars: Morphodynamic modeling based on characteristic dissipative Galerkin scheme. *Journal of Geophysical Research: Earth Surface*, *116*(3), 1–20. https://doi.org/10.1029/2010JF001941

Zhang, L., Parker, G., Stark, C. P., Inoue, T., Viparelli, E., Fu, X., & Izumi, N. (2015). Macro-roughness model of bedrock-alluvial river morphodynamics. *Earth Surface Dynamics*, *3*(1), 113–138. https://doi.org/10.5194/esurf-3-113-2015

Zhang, Li, Iwasaki, T., Li, T., Fu, X., Wang, G., & Parker, G. (2019). Bedrock-alluvial streams with knickpoint and plunge pool that migrate upstream with permanent form. *Scientific Reports*, *9*(1), 1–9. https://doi.org/10.1038/s41598-019-42389-2

Zhang, Li, Stark, C., Schumer, R., Kwang, J., Li, T., Fu, X., Wang, G., & Parker, G. (2018). The Advective-Diffusive Morphodynamics of Mixed Bedrock-Alluvial Rivers Subjected to Spatiotemporally Varying Sediment Supply. *Journal of Geophysical Research: Earth Surface*, *123*(8), 1731–1755. https://doi.org/10.1029/2017JF004431